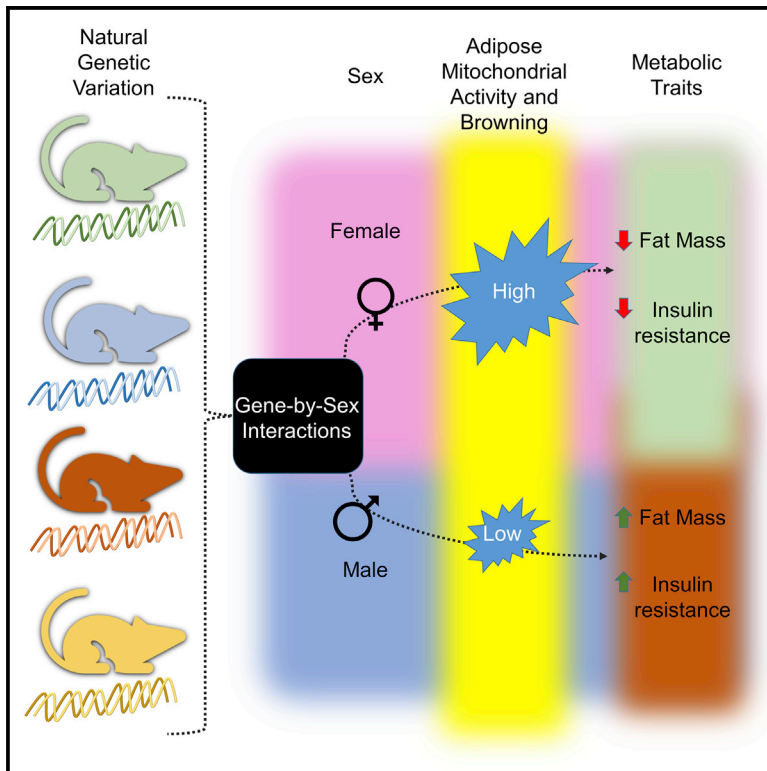


Cell Metabolism

Gene-by-Sex Interactions in Mitochondrial Functions and Cardio-Metabolic Traits

Graphical Abstract



Authors

Frode Norheim,
Yehudit Hasin-Brumshtein,
Laurent Vergnes, ...,
Susanna M. Hofmann, Arthur P. Arnold,
Aldons J. Lusis

Correspondence

jlusis@mednet.ucla.edu

In Brief

Norheim and colleagues use the hybrid mouse diversity panel to comprehensively address the role of sex, and its interaction with genetic background, on cardio-metabolic phenotypes and gene expression. They discover a sex-specific obesity locus for *Lyp1a1*, reveal sex-specific regulation of adipose tissue beiging, and find gene-by-sex interactions for mitochondrial function.

Highlights

- Sex differences in phenotype and gene expression depend upon genetic background
- The gene *Lyp1a1* impacts obesity in a sex-specific manner
- Functional analyses reveal sex differences for adipose tissue beiging
- Adipose mitochondrial function depends upon gene-by-sex interactions

Gene-by-Sex Interactions in Mitochondrial Functions and Cardio-Metabolic Traits

Frode Norheim,^{1,2,11} Yehudit Hasin-Brumshtein,^{1,11} Laurent Vergnes,³ Karthickeyan Chella Krishnan,¹ Calvin Pan,¹ Marcus M. Seldin,¹ Simon T. Hui,¹ Margarete Mehrabian,¹ Zhiqiang Zhou,¹ Sonul Gupta,¹ Brian W. Parks,⁴ Axel Walch,⁵ Karen Reue,³ Susanna M. Hofmann,^{6,7,8} Arthur P. Arnold,⁹ and Aldons J. Lusis^{1,3,10,12,*}

¹Department of Medicine/Division of Cardiology and Department of Human Genetics, University of California, Los Angeles, Los Angeles, CA, USA

²Department of Nutrition, Institute of Basic Medical Sciences, Faculty of Medicine, University of Oslo, Oslo, Norway

³Department of Human Genetics, University of California, Los Angeles, Los Angeles, CA, USA

⁴Department of Nutritional Sciences, University of Wisconsin-Madison, Madison, WI, USA

⁵Research Unit Analytical Pathology, Helmholtz Zentrum München, Neuherberg, Germany

⁶Institute of Diabetes and Regeneration Research, Helmholtz Zentrum Muenchen, German Research Center for Environmental Health (GmbH), Neuherberg, Germany

⁷German Center for Diabetes Research (DZD), Neuherberg, München 80336, Germany

⁸Medizinische Klinik und Poliklinik IV, Klinikum der Ludwig Maximilian Universität (LMU), Munich, Germany

⁹Department of Integrative Biology and Physiology, University of California, Los Angeles, Los Angeles, CA, USA

¹⁰Department of Microbiology, Immunology and Molecular Genetics, University of California, Los Angeles, Los Angeles, CA, USA

¹¹These authors contributed equally

¹²Lead Contact

*Correspondence: jlusis@mednet.ucla.edu

<https://doi.org/10.1016/j.cmet.2018.12.013>

SUMMARY

We studied sex differences in over 50 cardio-metabolic traits in a panel of 100 diverse inbred strains of mice. The results clearly showed that the effects of sex on both clinical phenotypes and gene expression depend on the genetic background. In support of this, genetic loci associated with the traits frequently showed sex specificity. For example, *Lyp1l1*, a gene implicated in human obesity, was shown to underlie a sex-specific locus for diet-induced obesity. Global gene expression analyses of tissues across the panel implicated adipose tissue “being” and mitochondrial functions in the sex differences. Isolated mitochondria showed gene-by-sex interactions in oxidative functions, such that some strains (C57BL/6J) showed similar function between sexes, whereas others (DBA/2J and A/J) showed increased function in females. Reduced adipose mitochondrial function in males as compared to females was associated with increased susceptibility to obesity and insulin resistance. Gonadectomy studies indicated that gonadal hormones acting in a tissue-specific manner were responsible in part for the sex differences.

INTRODUCTION

Sex differences in susceptibility to obesity, insulin resistance, and other cardio-metabolic traits have been amply described in mice, humans, and other species, with females generally ex-

hibiting beneficial metabolic profiles (Karp et al., 2017; Kenney-Hunt et al., 2008; Mittelstrass et al., 2011; Ober et al., 2008; Parks et al., 2015; Varlamov et al., 2014; White and Tchoukalova, 2014; Yang et al., 2006). Sex differences have also recently been identified for the gut microbiome (Fields et al., 2017; Org et al., 2016). Gene expression studies show that a large proportion of genes are differentially expressed in adipose, liver, brain, and other tissues (Della Torre et al., 2018; Kwekel et al., 2017; Yang et al., 2006) and that sex hormones as well as chromosome complement play a major role in modulation of gene expression (Kukurba et al., 2016; Mozhui et al., 2012; Rinn and Snyder, 2005; Vieira Potter et al., 2012; Yang et al., 2006). Directly or indirectly, sex differences arise from different sex chromosome dosage and can be either permanent or reversible in nature. Sex hormones contribute to both of these effects, but sex differences also arise independently of gonadal hormones because of sex-biased effects of X and Y chromosomes within cells (gene dosage, incomplete dosage compensation, and epigenetic effects) (Arnold, 2009; Arnold and Lusis, 2012; Bouret, 2013; Capel, 2017; Charlesworth, 1996; Chen et al., 2012; Disteche, 2012; Hager et al., 2008; Link et al., 2013; Link and Reue, 2017; McCarthy et al., 2009). For example, recent studies suggest that the sex chromosome complement plays a role in diet-induced obesity (Link et al., 2013; Traglia et al., 2017).

The vast majority of previous studies examined sex differences in phenotypes, genetic susceptibility to disease, or gene expression in isolation, generating trait- or tissue-specific results without putting them in context of genetic variation and network organization. In addition, only a few studies examined whether the observed differences are permanent or reversible in nature (Gregg et al., 2010; Hager et al., 2008; van Nas et al., 2009). In this work, we set out to examine the effect of sex on cardio-metabolic phenotypes in mice, with respect to phenotype-phenotype correlations, their genetic architecture, and the

underlying expression networks in adipose and liver. To examine gene-by-sex interactions, we performed our analyses with a panel of over 100 inbred strains of mice, known as the hybrid mouse diversity panel (HMDP). We demonstrate that not only do specific phenotypes differ between male and female mice, but the interdependencies between phenotypes, as well as the underlying genetic and molecular pathways are distinct. Our analysis of gene expression in adipose and liver shows that sex effects are highly tissue specific. Although effect sizes on gene expression are modest, they affect thousands of genes in each tissue and are physiologically relevant, as exemplified by our *Lyp1l1* knockout model. To understand the nature of the tissue-specific effect of sex, we examined liver and adipose expression in gonadectomized mice and observed that while the sex effects on gene expression in liver are largely reversible, those in adipose are not. Global expression data across the HMDP suggested that mitochondrial functions in adipose are a major contributing factor to the sex differences in metabolic phenotypes. To examine the underlying mechanisms, we isolated mitochondria from a subset of the HMDP strains and observed striking gene-by-sex interactions affecting respiration and electron transport chain complexes. Sex differences in metabolic traits were highly tissue specific. For example, we showed that while gonadal hormones have broad effects on gene expression in liver, their effects in adipose are much more modest. Our results indicate that gene-by-sex interactions are prevalent in cardio-metabolic traits in mice and that the differences are due in part to the effects on mitochondrial functions.

RESULTS

Study Design

Sex differences in experimental organisms, including mouse, have generally been studied on a single genetic background or in a cross between two strains. Our goal was to study sex differences in the context of genetic variation, so that we could examine interactions between genetic background and sex. Therefore, we selected the HMDP, a cohort of >100 inbred and recombinant inbred mouse strains that allows high-resolution genetic mapping (Bennett et al., 2010). The renewable nature of HMDP facilitates prospective collection of data on genetically identical individuals, thus making the comparisons between different conditions or over time feasible. The HMDP mice have been studied under a variety of dietary or other environmental conditions, and significant sex differences were observed in all of these studies (Lusis et al., 2016). The present studies are focused primarily on HMDP fed a high-fat, high-sucrose (HF/HS) diet (hfHMDP) that was previously described in detail by Parks et al. (Parks et al., 2013, 2015). The diet was chosen for its similarity to a typical western diet and relevance to metabolic disorders in human populations. Briefly, it includes 3 to 15 mice per sex from each of the 100 strains that were fed HF/HS diet for 8 weeks, between 8 and 16 weeks of age. Throughout the diet, as well as at the end of the diet, multiple phenotypes were measured (Table S1). It was not feasible in such a large study to collect data on female mice at a particular part of the estrous cycle, and we note that the reproductive phase can have a significant impact on metabolic traits, thereby contributing to non-genetic variation in female mice (Byers et al.,

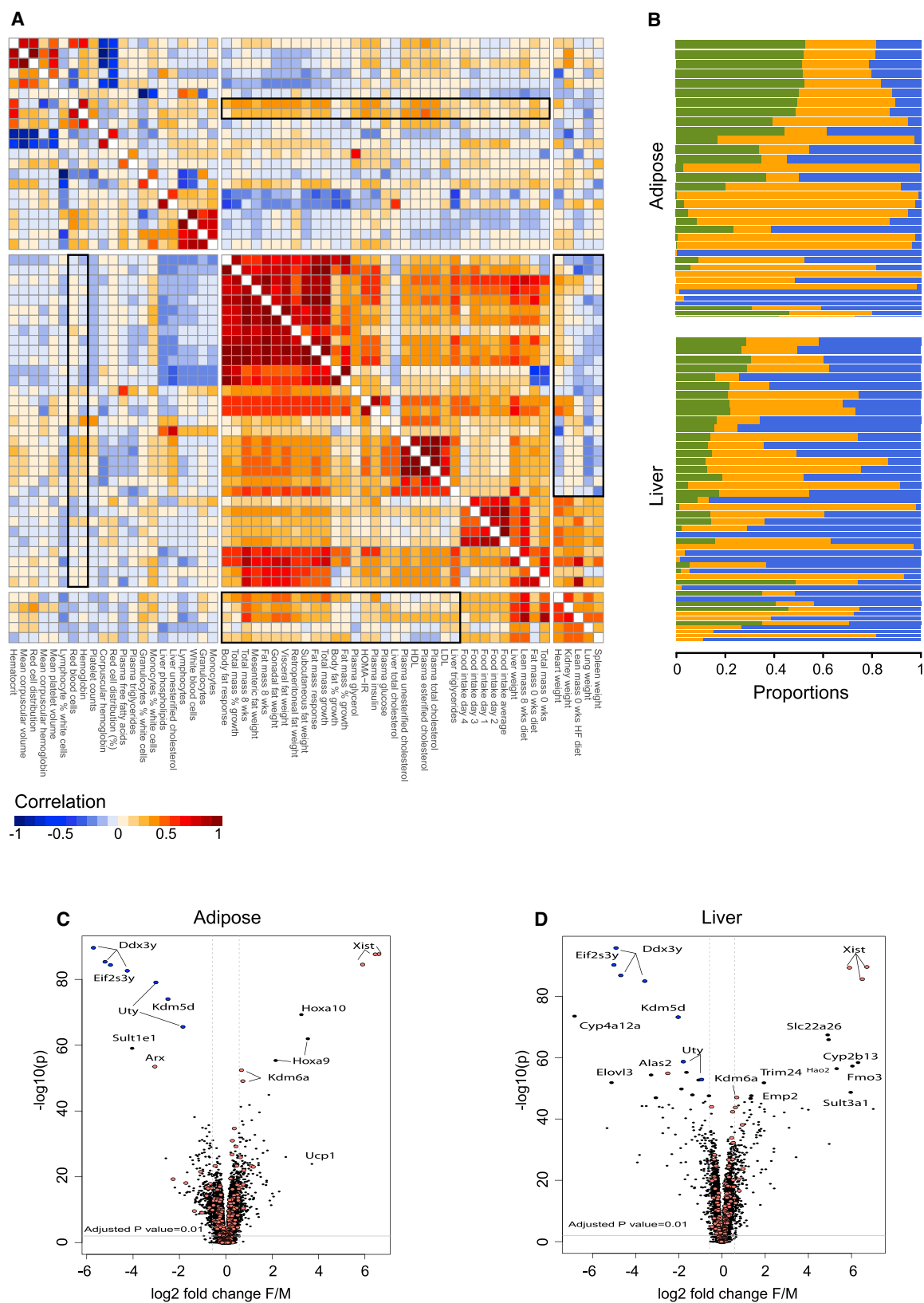
2012). We used expression microarrays to profile gene expression in the liver and gonadal adipose tissue of the individual mice. From a total of over 150 phenotypes examined in the hfHMDP study, we selected 59 that represented clinically significant traits such as insulin resistance, obesity, plasma lipids, and fatty liver disease (Table S1). Finally, we tested hypotheses generated by our analyses using engineered models, functional studies of isolated mitochondria, or gonadectomy experiments on a more limited set of genetic backgrounds.

Sex Differences Affect Interdependencies of Phenotypes, Gene Expression, and Phenotype-Transcript Correlations

Correlation between two phenotypic measurements implies either common underlying factors or a direct dependency between the phenotypes. In addition, when one phenotype is easily measurable while the other is not, closely correlated phenotypes are often used as proxy for one another. An important question is not only whether the phenotype itself shows sex differences but also what parts of the phenotypic networks are sex specific. Thus, we explored whether sex affects the correlation structure between phenotypes and whether the underlying associated molecular pathways are similar between sexes. To this end, we examined sex-specific phenotype-phenotype correlations on three levels, (1) inter-sex phenotype-phenotype correlations (Figure 1A), (2) co-sharing of genes where expression is significantly associated with the phenotype in liver or adipose tissues (Figure 1B), and (3) tissue-specific patterns in sex-dimorphic gene expression (Figures 1C and 1D).

The examined phenotypes from hfHMDP broadly represent four categories—blood-related phenotypes (such as blood cell counts and percentages), body mass related (such as total body mass, organ weights, lean and fat masses, and growth), behavioral (food intake), and metabolic (glucose and insulin measurements, liver and plasma cholesterol). As expected, we find a profound sex difference in all body mass-related phenotypes, which could mostly be attributed to differences in body size (Table S1). Once corrected for body size (using kidney weight; STAR Methods) these differences were no longer significant. We note that this is not a perfect way to adjust and that kidney weight could also be affected by sex differences. With the exception of granulocyte cell counts, blood-related phenotypes showed no significant sex differences, consistent with previous observations in mice and humans (Karp et al., 2017). However, all of the metabolic phenotypes as well as food intake showed a profound sex difference (Table S1). Notably, although stratified body fat (BF) increase and weight gain were similar in males and females, stratified food intake was significantly higher in the females, suggesting differences in basic energy expenditure between sexes.

We compared phenotypes in males and females using pairwise bi-weight mid-correlations (a median-based measure that is less sensitive to outliers than Pearson correlations) (Figure 1A). As many of the phenotypes are not independent, and some are mathematical derivations of others (e.g., BF percent increase is derived from total mass and fat mass), to evaluate significance we computed 1,000 permutations for each pairwise comparison (>3 million permutations in total). The permuted distributions were similar between the sexes and phenotype pairs and suggested that correlations stronger than 0.25 correspond to p value



(legend on next page)

threshold of 0.01, whereas those stronger than 0.34 correspond to p value of $1e-3$. A heatmap of the pairwise correlations between all phenotypes in males and females (Figure 1A) shows that, as expected, the strong pairwise correlations are generally replicated between sexes. Yet, we could also identify differences in the correlation structure where a set of correlations was notably different (Figure 1A, emphasis boxes). For example, in males, the lean mass before HF/HS diet and spleen and lung weights after 8 weeks of diet are negatively correlated to most measures of body fat and cholesterol, whereas in females, these correlations are mostly positive (rightmost versus middle bottom emphasis box, Figure 1A). An opposite disparity was observed for correlations between red blood cell counts or hemoglobin measures to metabolic phenotypes and food intake (upper and leftmost emphasis boxes, Figure 1A). Figure S1 shows detailed plots of correlations for selected phenotypes in highlighted areas in Figure 1A.

Another way to assess similarity between molecular pathways underlying or affected by phenotypes is by shared effects on gene expression. Thus, we examined the overlap between genes whose expression is associated with each phenotype in males and females using global gene expression data from liver and gonadal adipose across the hfHMDP. We picked all genes that were associated with each of the phenotypes, in either sex or tissue, at the $p < 1e-6$ level (a permutation-based threshold for phenotype-transcript associations in HMDP equivalent to false discovery rate [FDR] = 0.01) and computed the overlap per tissue per trait (Table S1). Figure 1B shows that the proportion of overlap varies between traits and tissues but generally does not exceed 50%.

Notably, in both tissues there are global sex effects on gene expression; thousands of genes show significant and robust, although modest, differential expression in either sex (Kukurba et al., 2016; Rinn et al., 2004; Rinn and Snyder, 2005; Roy and Chatterjee, 1983; van Nas et al., 2009; Yang et al., 2006). To analyze differential expression in the hfHMDP microarray data, we filtered out probes based on technical quality parameters (such as identity to target sequence or uniqueness; see STAR Methods for details) and prevalence of expression (intensity >4 in >75 strains in either sex). We then tested 8,673 genes in adipose and 7,235 genes in liver for sex differences in expression. Our model ($= \sim \text{strain} + \text{sex}$) included blocking on strain identity, a conservative option for multiple testing correction and adjusted p value threshold of 0.01 (STAR Methods). Consistent with previous observations, we identified sex differences in expression of thousands of genes in either tissue (3,948 in adipose and 3,719 in liver; Figures 1C and 1D) and significant overlap between the tissues (1,608 regulated in both tissues, chi-square = 39.6, $p = 3e-10$). While our results are generally consistent with previous studies, our estimates of differentially

expressed genes are notably higher. The higher estimation in our study likely stems from both the technical differences (our analysis includes more strains and mice, resulting in higher power) and differences in the experimental setup (the sex influence on gene expression in our study may be amplified indirectly by the different response to the HF diet). In addition, our WGCNA analysis of co-expression networks in both sexes shows module preservation of the very large co-expression modules that reflect basic cellular function but not the smaller ones representing specific biologic processes (data not shown).

We further explored what potentially functional aspects of adipose and liver biology are reflected by the genes that are differentially expressed between the sexes (Tables S3 and S4) and the role of sex hormones in regulating these differences. Enrichment analysis (Table S3) clearly shows an upregulation of genes involved in mitochondrial function in the adipose tissue of females relative to males. Terms and pathways that were highly enriched included “mitochondrion” ($p < 1e-25$), “mitochondria inner membrane” ($p < 1e-11$), “oxidative phosphorylation” ($p < 1e-14$), electron transport ($p < 1e-12$), respiratory chain ($p < 1e-11$), and mitochondrial matrix ($p < 1e-7$); all were highly significant after Benjamini-Hochberg correction. Practically all genes in the mitochondrial oxidative phosphorylation pathways showed significantly higher expression in female adipose tissues (data not shown).

Sex Differences Have Strong Effects on Cardiovascular and Metabolic Traits and Are Affected by Genetic Background

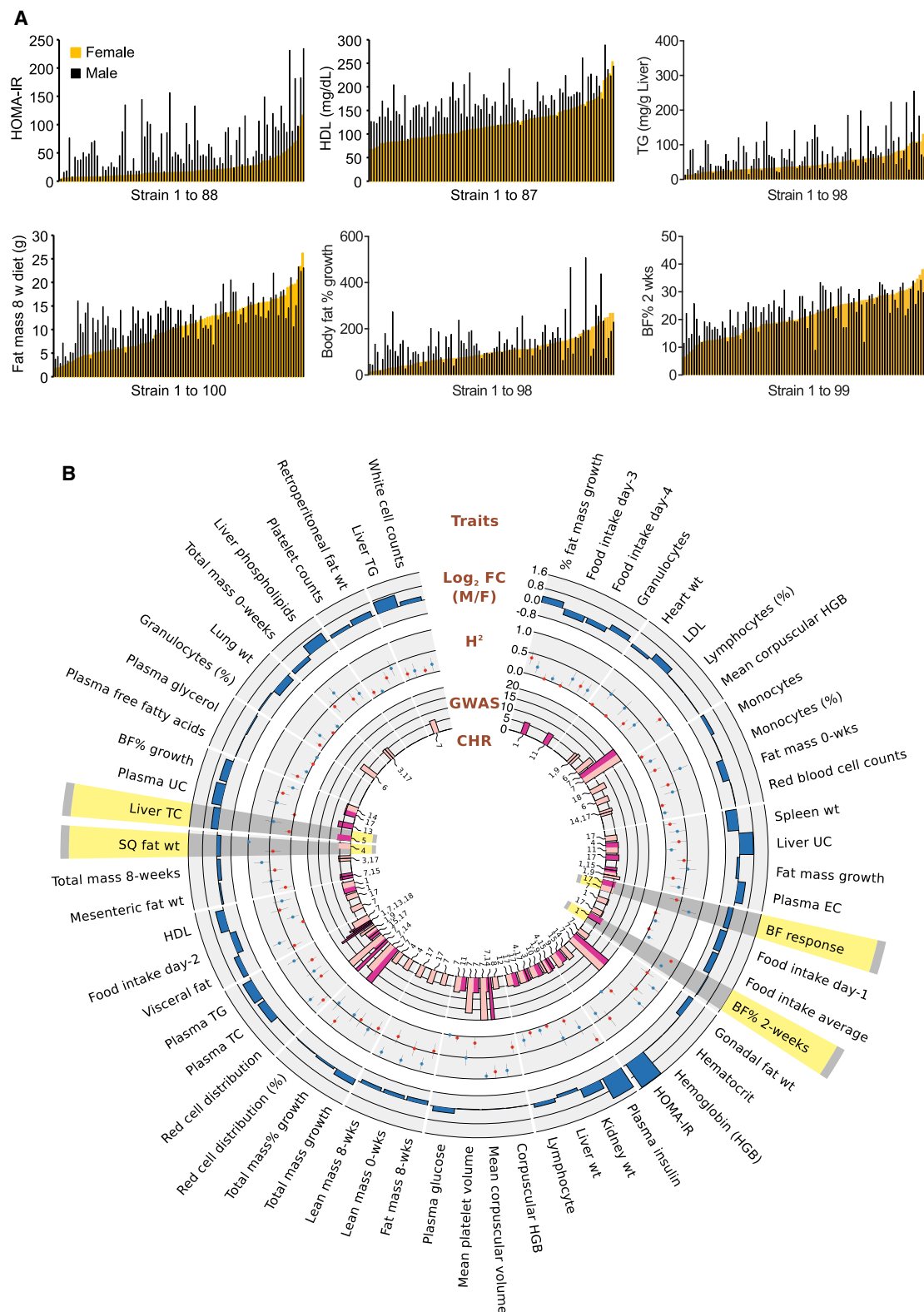
Previous studies with the HMDP examined phenotypes in male and female mice under a variety of diets and other environmental conditions. These studies showed profound sex differences in metabolic phenotypes related to obesity (both on chow and HF diets), insulin resistance, fatty liver, plasma lipids, atherosclerosis, and gut microbiota (Lusis et al., 2016). In some cases, such as insulin resistance (Figure 2A) and atherosclerosis, one sex is much more susceptible than the other, whereas in other cases the differences are more modest. Yet in all cases, the genetic background appears to perturb the sex differences and sometimes even reverse them, exemplifying abundant gene-by-sex interaction ($G \times S$) in the metabolic phenotypes. Figure 2A and Table S2 show examples of six phenotypes in hfHMDP (HOMA-IR, HDL, plasma TG, fat mass, body fat % growth, and body fat % after 2 weeks of diet) that not only show sex differences across strains but also exemplify the substantial effect of genetic background on the sex differences.

Sex-Specific Loci in Genome-wide Association Studies

To examine the extent to which mapping of traits overlaps between males and females, we remapped all QTL loci identified

Figure 1. Cardio-Metabolic Traits Exhibit Sex-Specific Interdependencies in Trait-Trait and Trait-Transcript Correlations

(A) Heatmap representing pairwise bi-weight mid-correlation between phenotypes in females (lower triangle) and males (upper triangle). Two areas of different correlation structure are highlighted with boxes. All HMDP strains for which the data were available have been included in this analysis.
(B) Proportion of overlap of transcripts associated ($p < 10^{-5}$) with phenotypes in both sexes in liver and adipose. Green indicates proportion of overlapping genes, while orange and blue show sex-specific associations for females and males, respectively. Bar width is proportional to \log_2 of number of genes associated with the trait in total (see Table S1 for phenotypes).
(C and D) Volcano plots of sex differences in expression in hfHMDP in the adipose (C) and liver (D). Horizontal gray lines indicate adjusted threshold of $p < 0.01$, vertical gray lines indicate a 2-fold difference. Genes residing on chromosomes X and Y are colored pink and blue, respectively.



(legend continued on next page)

by genome-wide association studies (GWASs) in males and females separately. Mapping was performed with FaST-LMM with correction for population structure using an FDR of about 1% as previously described (Bennett et al., 2010; Lusi et al., 2016; Parks et al., 2013, 2015). Among the 59 traits, we were able to map significant loci for 49. Many of these loci exhibited significant association in one sex only. In typical GWASs carried out in humans or linkage studies in outbred or F2 mouse crosses, limiting the analyses to one sex would cause a significant loss of power because it would reduce the number of recombination events encompassed by each cohort. However, in the HMDP, both male and female cohorts represent the same strains and, thus, the same compendium of genotypes and recombination events. Therefore, in this setting, sex segregation only affects the mapping power to the extent that it affects the accuracy of average strain phenotype value. This can in turn reduce, improve, or have no notable effect on the accuracy of GWAS mapping, depending on the number of mice in each group, the variance of the phenotype within each sex, and the true difference in phenotype mean between the sexes. Since sex differences in phenotypes are prevalent and significant (Table S1), it stands to reason that segregating the analysis by sex will potentially increase the power to map loci.

Overlap of GWAS loci can be assessed at various resolutions. While HMDP mapping resolution is typically ~3 Mb, locus-specific linkage disequilibrium (LD) structure can produce substantial long-range effects and wide mapping peaks. Thus, it is not always clear if two peaks on the same chromosome truly represent distinct QTLs. Therefore, in this analysis, we counted an overlap if a locus resides on the same chromosome in both sexes, which in our opinion represents the lowest, most conservative estimate of overlap. Surprisingly, even at this resolution, we clearly see that a majority of QTLs do not overlap between sexes, even if we only consider traits that map in both sexes (Figure 2B). Consistent with the idea of genetic effects on sex specificity of phenotypes, we observe clustering of sex-specific loci for multiple traits. For example, loci on chromosome 17 contribute to multiple fat mass-related phenotypes in males (Figure 2B), and QTL on chromosome 15 contributes to HOMA-IR and cholesterol levels only in females, while the same traits were mapped to chromosome 9 in males. In contrast, 7 out of 10 common traits mapped to chromosome 7 in both sexes (Figure 2B). Importantly, lack of overlap among loci can also be affected by threshold effect—i.e., a locus may just pass the significance threshold in one sex and approach it in another. Undoubtedly, some of the identified sex-specific loci reflect differences in effect size between males and females. However, some of the loci show a strong association in one sex and no evidence of association in the other (see examples in Figures 2B, 3, and 4).

Sex-specific estimates of broad-sense heritability (H^2 ; Figure 2B) also suggest that there is substantial sex specificity in genetic contribution to the observed variance in our phenotypes. It is noteworthy that for many of the traits measured, heritability

was lower in females than males. It is likely that this is explained in part by the reproductive phase of females. As discussed above, it was not feasible to control for the reproductive cycling of females in our study. This additional noise in females would also impact the strength of association in GWASs.

Systems Genetics Approach Elucidates Sex-Specific Loci of Clinical Traits

Given that we observed striking sex-specific differences in phenotypic traits and consequent heritability measures, we next searched for genetic loci that significantly associate to clinical traits exclusive to one sex. Therefore, genome-wide significant ($p < 4.1 \times 10^{-6}$) SNPs, which map to relevant traits (above), were obtained for one sex and filtered for the entire chromosome being below this threshold in the other (some examples are highlighted in Figure 3). These would reflect loci for indicated clinical traits, whereby the candidate regions are exclusively observed in only one sex. Initially, we filtered the peak SNPs for these loci for those which are also *cis*-eQTLs for adipose tissue genes. Upon examination of the *cis*-eQTLs and correlations in both sexes, we thought it best to make less assertive conclusions regarding which specific genes could underlie this sex-specific response. One consideration in using *cis*-eQTL to prioritize candidate genes is that in general, only a small fraction of total variation in gene expression is explained in *cis*. Given that there are a substantial number of genes within these regions which are also *cis*-eQTLs for expression in adipose tissue (or liver) and that, in general, *cis*-regulation of gene expression explains a very small fraction of the variance, all proximal genes are shown in Figure 3. Here, we provide several potential candidates that could play important roles depending on the tissue and sex. Collectively, we are able to demonstrate several notable gene-by-sex interactions through identification of genetic loci, which are likely driving variations in cardio-metabolic traits predominantly in one sex.

Validation of a Gene Polymorphism Affecting Response to a High-Fat Diet in Females, but Not Males: *Lyplal1*

The BF% in the hfHMDP was measured bi-weekly over 8 weeks of diet. Association mapping of BF% after 2 weeks of an HF/HS diet revealed a female-specific locus on chromosome 1 (Figure 4A). This locus encompassed only one gene, *Lyplal1*, which is also a GWAS candidate in human obesity studies (Heid et al., 2010; Lindgren et al., 2009). *Lyplal1* has a deleterious missense mutation rs31134248 (I58T, as predicted by the PROVEAN prediction algorithm; Figure 4B) (Choi and Chan, 2015), which is also the strongest local (and presumably *cis*-acting) expression quantitative trait locus (local-eQTL) in adipose tissue of males ($p = 3 \times 10^{-20}$), whereas in females, the strongest local-eQTL is rs32885362 ($p = 1.44 \times 10^{-25}$; Figure 4C). Both of these SNPs reside close to each other and are in high linkage disequilibrium.

To investigate potential mechanisms underlying the sex difference, we compared *Lyplal1* expression between the sexes.

(B) Circos plot showing an overview of sex-specific regulation of clinical traits. The outermost track (blue bars) show the relative \log_2 fold change (FC) across all strains (male versus female). The middle track represents heritability estimates for the metabolic traits in females (red) and males (blue). Bars indicate 95% confidence interval. The innermost track represents $-\log_{10}$ p value (capped at 20) of notable GWAS loci in females (dark pink) and males (light pink), with their respective genome positions indicated below the bars. Bars indicate significant ($p < 4.1 \times 10^{-6}$) mapping. Examples of sex-specific traits are highlighted and are discussed in detail in Figures 3 and 4.

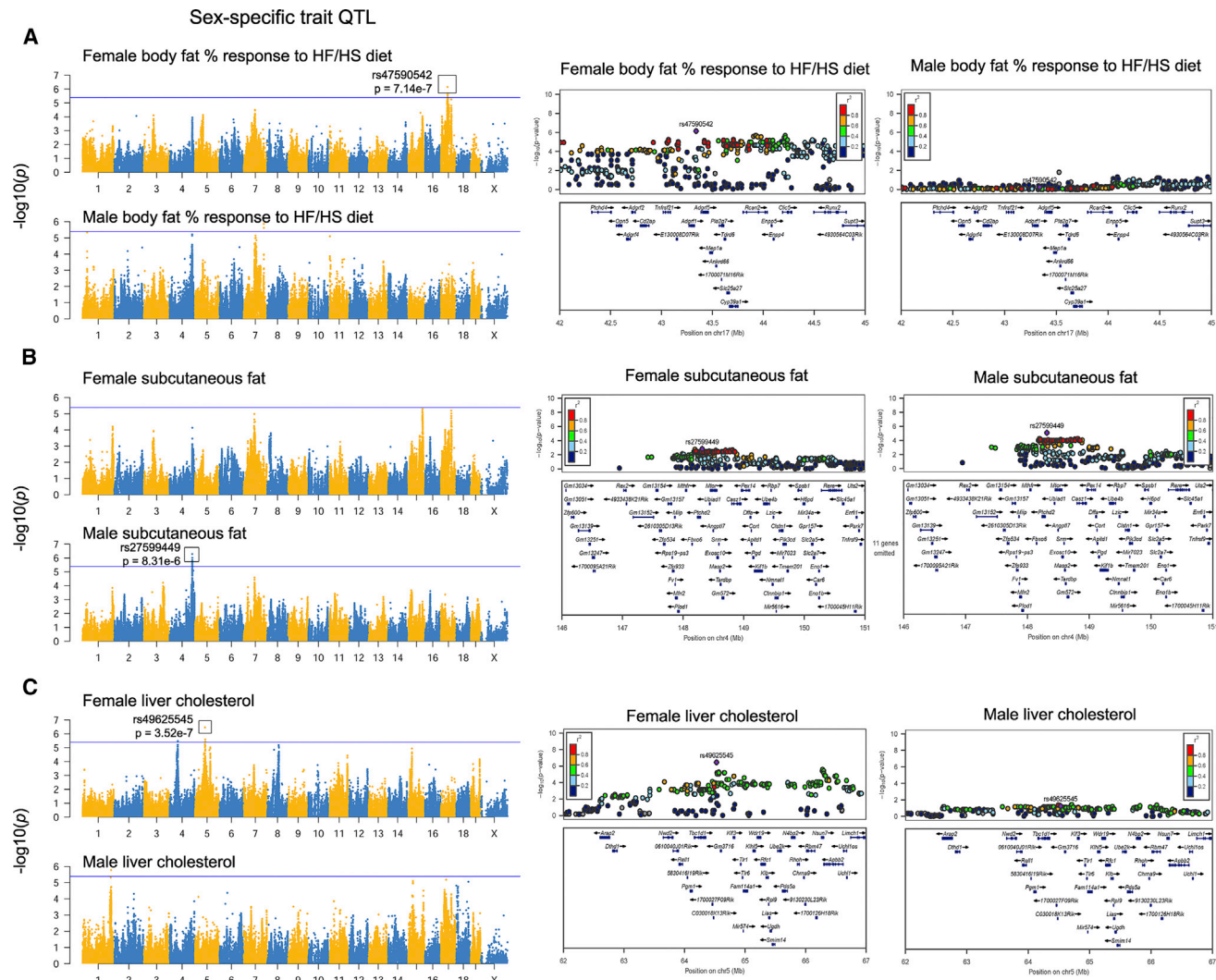


Figure 3. Sex-Specific Genetic Loci for Clinical Traits

Examples of sex-specific, genome-wide significant loci (left) and LocusZoom plots for the indicated peak SNP in female (middle) or male (right) body fat % response to HF/HS diet (A), subcutaneous fat pad weight (B), and liver cholesterol (C). Bars indicate significant ($p < 4.1 \times 10^{-6}$) mapping.

Females showed significantly higher adipose *Lyplal1* expression levels than males ($p = 6.47 \times 10^{-47}$; Figure 4D). Furthermore, females, but not males, showed a significant negative correlation between adipose *Lyplal1* expression and BF% after 2 weeks of HF/HS feeding (Figure 4E). Moreover, the SNP coding for the detrimental missense mutation (rs31134248) showed a significant association with BF% after 2 weeks of HF/HS diet in females ($p = 2 \times 10^{-4}$), but not in males ($p = 0.53$). Pathway enrichment analysis of the genes correlating most strongly with *Lyplal1* expression in female adipose tissue revealed significant enrichment for genes involved in oxidation and mitochondria (Figure S2A). Similar pathway enrichment for *Lyplal1* was observed in male adipose tissue (data not shown).

To test whether variation in *Lyplal1* underlies the BF phenotype, we studied whole body knockout (KO) mice for *Lyplal1* in strain C57BL/6N mice (C57BL/6J and C57BL/6N are closely related substrains). In order to replicate the conditions of the to

hfHMDP, the *Lyplal1* KO, heterozygous (Het) and wild-type (WT) mice were fed a HF/HS diet for 2 weeks and their BF% was monitored before and after the study. Consistent with the dietary and sex specificity of the GWAS loci, we observed no difference in BF% among the three genotypes at baseline (0 week of HF/HS) when fed a chow diet. After 2 weeks of HF/HS diet, the female KO mice showed a significant higher BF% than both the WT and Het mice taken together (Figure 4F). This was not observed in male mice (Figure 4F). A similar female-specific difference in the KO mice (compared to Het and WT mice) was observed for BF% growth at the same time point (Figure 4G). These observations indicate that *Lyplal1* has a protective effect uniquely in females against the fat mass gain in response to switching to an HF/HS diet. We note that strain C57BL/6J mice are not unusual in the level of expression of *Lyplal1* in adipose, with levels that are average (males) or slightly below average (females) as compared to the other HMDP strains (Figure S2B).

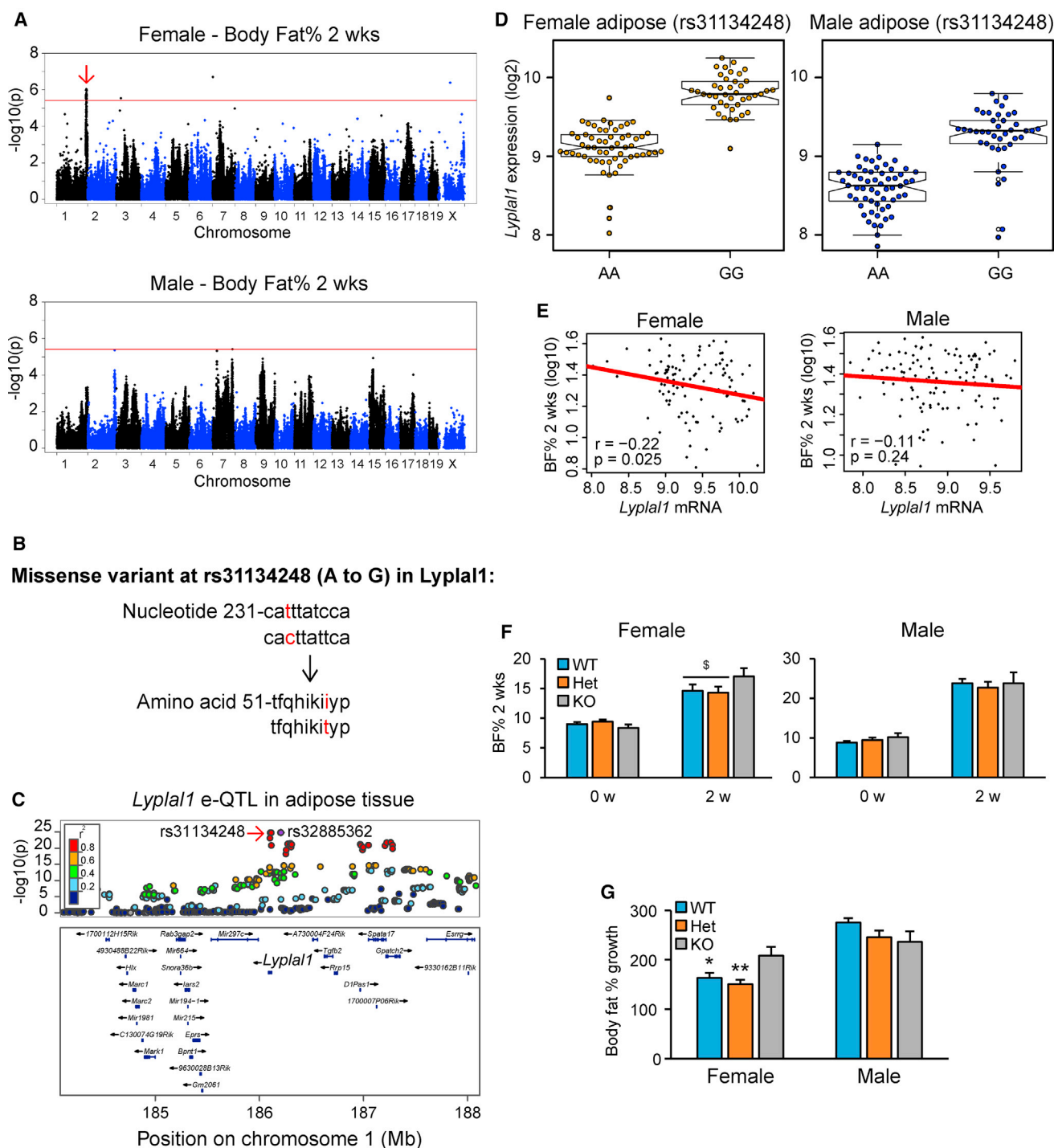


Figure 4. *Lyplal1* Exhibits a Sex-Specific Gene-by-Diet Effect on Body Fat % Growth

(A) Manhattan plot showing the significance ($-\log_{10}$ of p value) of all SNPs and body fat percentage after 2 weeks of HF/HS feeding in female and male hfhMDP mice. Chromosome 1 locus containing the *Lyplal1* gene is indicated with an arrow. The genome-wide significant threshold (red) of $p = 4.1 \times 10^{-6}$ is indicated. GWAS was performed on \log_{10} -transformed data to achieve a normal distribution.

(B) Missense variant at rs31134248 (A–G) in the *Lyplal1* gene. The resulting changes in nucleotide and amino acid sequences are depicted in red letters.

(C) LocusZoom plot for cis-eQTL associations between *Lyplal1* expression and the nearby SNPs at chromosome 1. The significant association ($-\log_{10}$ of p value) between SNPs and *Lyplal1* are depicted. The degree of correlation between the SNP correlating the most with *Lyplal1* (rs3288536) and all other SNPs are shown. The missense variant (rs31134248) is depicted.

(D) *Lyplal1* expression in female and male adipose tissue in hfhMDP for the two missense alleles (rs31134248).

(E) Correlation of adipose gene expression of *Lyplal1* with body fat percentage after 2 weeks of HF/HS diet in female and male hfhMDP mice.

(legend continued on next page)

Gonadectomy Studies Indicate that Gonadal Hormones Largely Account for Sex Differences in Adult Liver, but Not Adipose

One molecular model of hormonal regulation of gene expression is based on binding of sex-biased transcription factors to DNA, similar to other regulating cascades. Sex specificity in this model arises from circulating levels of gonadal hormones and consequently may be thought of in general terms—i.e., if a gene is regulated, for example, by estrogens in one tissue, it is likely to be regulated by estrogens in other tissues as long as the tissues express one of the estrogen receptors. Few explicit examples of tissue-specific regulation of particular genes by gonadal hormones (or tissue-by-sex interactions) have been described, but to the best of our knowledge no studies so far have examined the overlap between tissues.

In this work, we compared the extent of sex regulation of gene expression between adipose and liver on both chow and HF/HS diets using gonadectomy (GDX) experiments. Both datasets clearly indicate prevalent tissue-by-sex interactions on regulation of gene expression. In intact mice, the first two principal component analysis (PCA) axes correspond, as expected, to sex and diet (Figure 5). However, PCA of intact and gonadectomized mice generated strikingly different trajectories of shift in gene expression in adipose and liver. Specifically, in liver, gonadectomy of males resulted in a shift in gene expression profile toward that of intact or gonadectomized females (PC1 in Figures 5B and S3A), while in adipose, the gonadectomized samples were not closer to the other sex (Figure 5A). First, these observations are consistent with previous studies of gonadectomized male mice with regard to liver transcriptional regulation (Jalouli et al., 2003), some of which could be reversed with hormone replacement (Falls et al., 1997; Tai et al., 2003). Second, with the exception of chromosome Y and several chromosome X genes, in both datasets there was no evident correlation between sex effects on gene expression in the adipose and liver (Figure 5C). To test whether the large shift in gene expression following gonadectomy in males was due to loss of testosterone, we carried out hormone replacement. Indeed, following testosterone (DHT) treatment, the expression of selected genes that contributed substantially to the variation in PC1 (Figure S6) affected by gonadectomy shifted back to intact levels (Figure 5E). This shows that genes that are driving the shifts in transcriptome following gonadectomy can be reversed following hormone replacement.

To examine the possibility that differences in gene expression between sexes or following gonadectomy were due to changes in cell composition, we performed deconvolution analyses. We used an existing deconvolution method (SaVanT, <http://newpathways.mcdm.ucla.edu/savant>) to assess cell-type composition of the adipose samples from the hfHMDP survey and the gonadectomy experiments. Based on gene expression, the primary component in all adipose samples consisted of adipo-

cytes across all groups (Figures 5F–5H), and there were no apparent differences in cell-type composition between the sexes or as a result of gonadectomy (Student's *t* test, *p* = 0.991).

Gene-by-Sex-by-Tissue Interactions Affecting Gene Expression

Next, we explored whether regulation of gene expression as a function of genetic background is shared between sexes. Genetic regulation of gene expression may manifest in a tissue- or sex-specific manner if, for example, the genetic variant affects a regulatory element active only in one tissue or sex. Tissue-specific regulation of gene expression is well documented in mouse and human eQTL studies, but the extent of gene-by-sex interactions is not well understood. To look at gene-by-sex and gene-by-tissue interactions, we compared the overlap in local eQTLs in both a tissue- and sex-specific manner (Figure 5D). Specifically, we generated four separate local-eQTL lists (within 5 Mb of the gene) for each tissue and sex and compared the overlaps of genes with local-eQTLs between those lists. To avoid biasing our counts by genes that are only expressed in one tissue, this analysis was limited to genes expressed in both adipose and liver tissues in at least one sex (i.e., the overlap of lists used for analysis of sex differences in the two tissues). We labeled the genes as “common” (those that have a local-eQTL in 3 or all 4 datasets), “liver” or “adipose” (those that have a local-eQTL only in liver or in adipose), “sex-specific” (detected in only one sex but in both tissues), and “reciprocal” (detected in one sex in one tissue but in another sex in the other tissue). We regarded the proportion of “reciprocal” set as an approximation of overlap that is independent of either sex or tissue. Notably, among all the genes that have local-eQTLs, 26%–32% were shared by both tissues, while 58%–64% were specific to either tissue. Within each tissue only ~50% of eQTLs were shared between sexes, and 50% were sex-specific—suggesting that gene-by-sex interactions are prevalent within a tissue context. In contrast to the abundance of sex-specific regulation in a tissue-specific context, the “sex-specific” and “reciprocal” groups were only 1%–2% of the genes, suggesting that cross-tissue gene-by-sex regulation of gene expression is very limited.

This analysis may be biased in two ways: first, eQTLs may be just above the threshold in one sex and below (for example, due to increased noise) it in the other. In such cases, one expects to see better overlap as the threshold becomes more and more stringent. The proportions of all groups remained stable across different *p* value thresholds for local-eQTLs (Figure 5D), suggesting that the results are not significantly affected by lower confidence data. Second, local eQTL lists could be biased by sex differences or tissue differences in total expression, in which case we would be more likely to detect sex-specific eQTLs in the higher-expressing sex or tissue. However, we did not observe inter-group differences in the average expression of the local-eQTL genes or in sex specificity of their expression (Figure S4).

(F) BF% both before and after 2 weeks of HF/HS diet in female and male wild-type (WT), heterozygotes (Het), and KO mice for *Lyp1l1*.

(G) BF% growth (0 to 2 weeks) in response to a HF/HS diet in female and male WT, Het, and KO *Lyp1l1* mice. The number of WT, Het, and KO mice studied was 28, 31, and 14, respectively, for females, and 30, 22, and 7, respectively, for males.

Results are presented as mean ± SEM. **p* < 0.05 and ***p* < 0.01 between the KO mice and either WT or Het mice. \$*p* < 0.05 between the KO mice and both the WT and Het mice. Statistics were performed on log-transformed data. *p* values were calculated using a Student's *t* test (two-way).

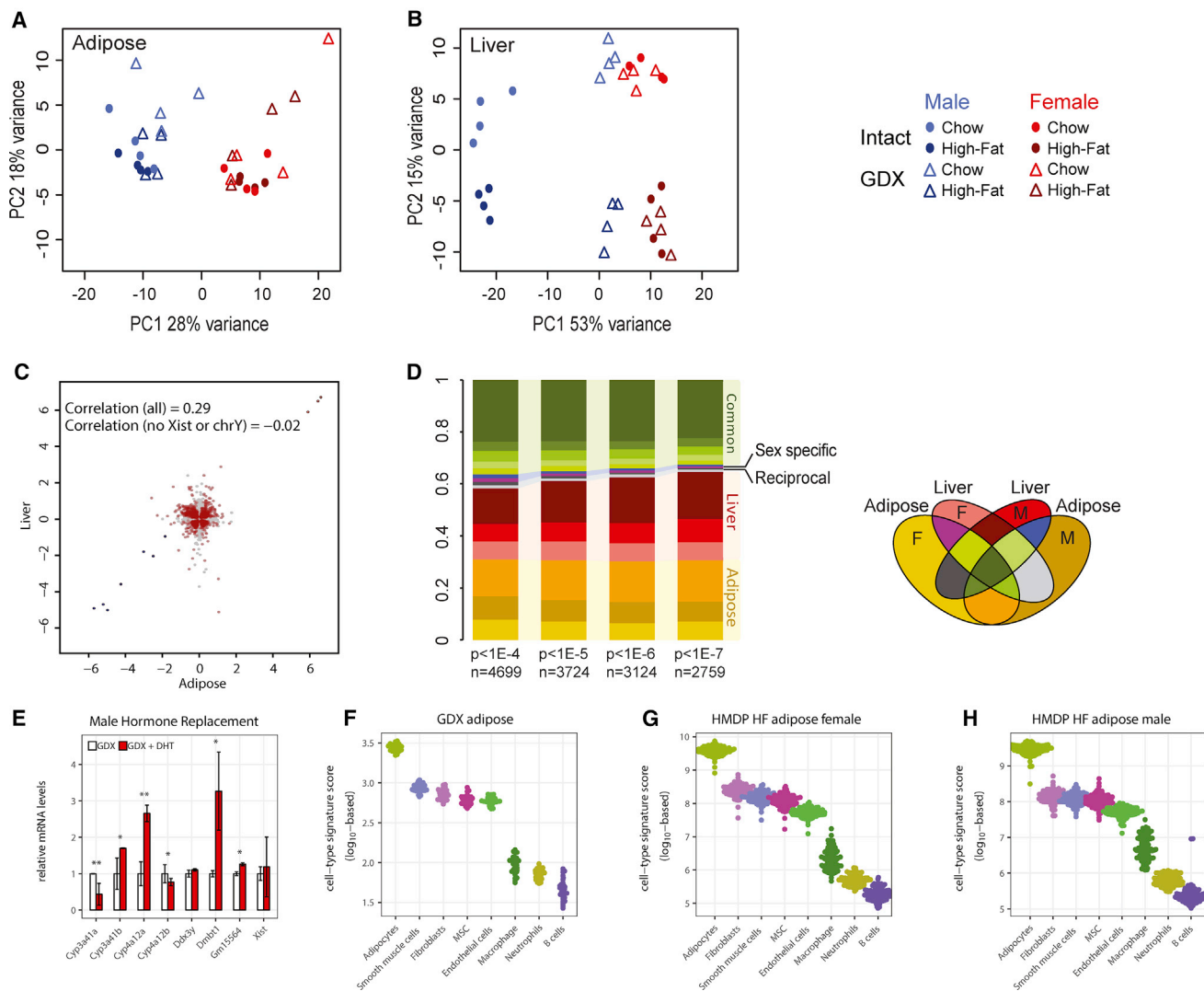


Figure 5. Tissue Specificity of Sex Differences in Regulation of Expression

(A and B) Total gene expression in adipose (A) and liver (B) was summarized using principal-component analysis (PCA), a data reduction method, in two dimensions for intact mice and gonadectomized mice. Note that the axes in liver and adipose are the same. Dots indicate intact samples, triangles indicate gonadectomy (GDX), males are in blue and females are in red, chow diet is in lighter color, and HF diet is darker. In control samples, PC1 in both tissues differentiates between sexes, while PC2 corresponds to diet.

(C) Plot of correlation between effects of gonadectomy in liver and adipose.

(D) Sex specificity of expression QTLs (eQTLs) in hfHMDP. eQTLs common to both tissues are in green, adipose specific are in yellow, liver specific are in red, reciprocal are in gray, and sex specific are magenta (females) and blue (males). Color legend on the right indicates the overlapping section of the four datasets. (E) Livers from gonadectomized C57BL/6J male mice with or without testosterone (DHT) pellet administration were analyzed for expression changes corresponding to the top 7 contributing genes to liver principal-component variation (shown in Figure S6). Five of the seven genes driving shifts in principal components were shifted back to levels similar to intact mice via hormone replacement.

(F–H) Adipose deconvolution from GDX experiments (F), HMDP HF/HS females (G), and HMDP HF/HS males (H).

Results are presented as mean \pm SEM. * $p < 0.05$ and ** $p < 0.01$ between gonadectomized males and gonadectomized males with testosterone implants (DHT). p values were calculated using a Student's t test (two-way), $n = 6$ per group, and expression normalized to the geometric mean of PPIA and RPL13a.

Global Sex Differences in Gene Expression Highlight Mitochondrial Function in the Adipose

Interestingly, and consistent with the enrichment analysis, one of the most significantly differentially expressed genes in adipose tissue was *Ucp1* (~ 25 -fold $F > M$, $p < 1e-17$; Figure 6A). *Ucp1* encodes uncoupling protein 1, a protein carrier in the inner mitochondrial membrane with an important physiological role in

thermogenesis through the dissipation of oxidation energy as heat. UCP1 activity is high in brown adipose tissue and may be induced under some conditions in white adipocytes (often known as adipose tissue “beiging”). Both of these are generally associated with an improved metabolic profile (Cannon and Nedergaard, 2004; Giordano et al., 2016). *Ucp1* expression in adipose tissue was significantly correlated with adipose-related

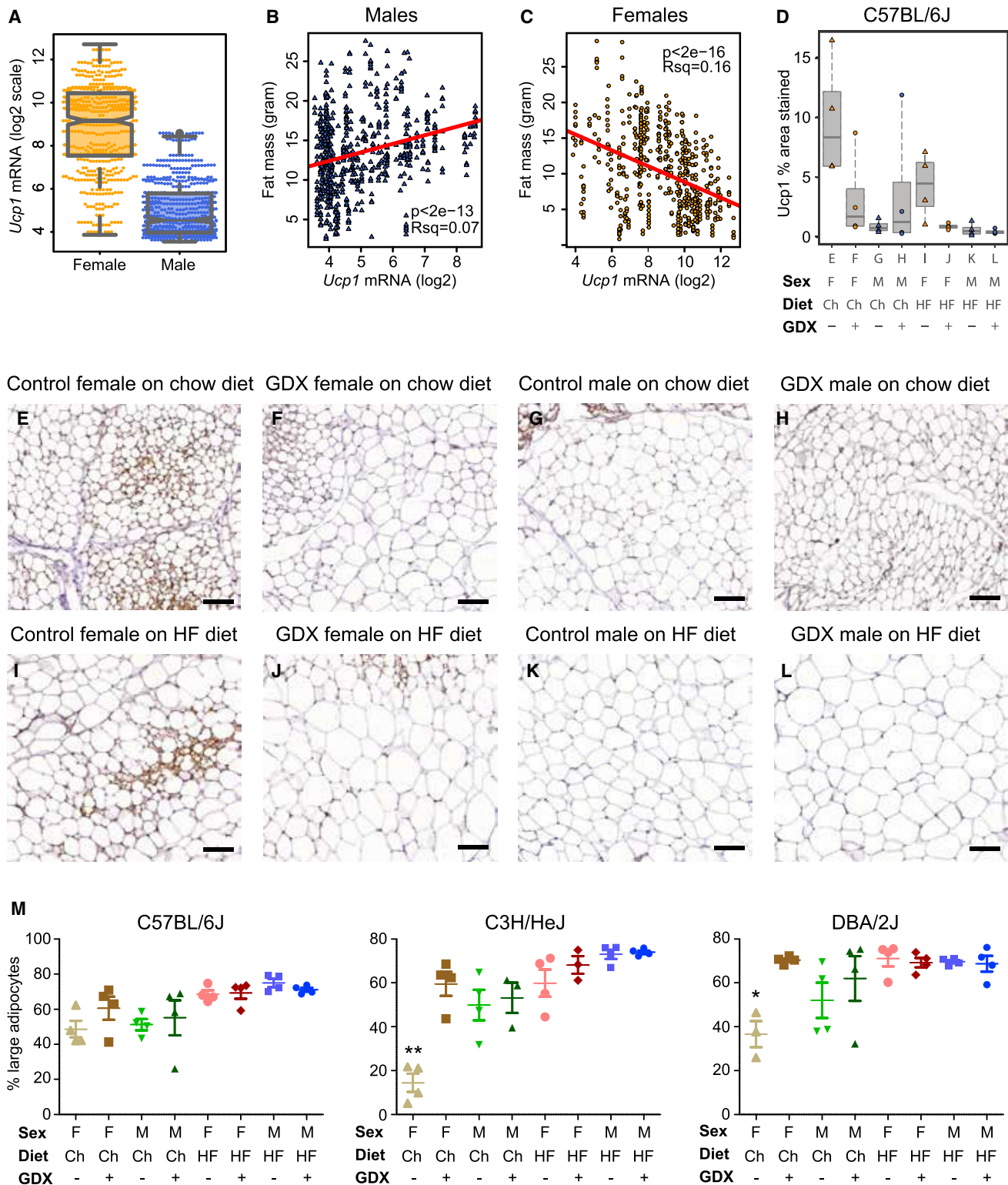


Figure 6. Sex Differences in Adipose Tissue Point to Mitochondrial Function

(A) *UCP1* expression in female and male adipose tissue in hFMDP.

(B and C) *UCP1* is significantly and inversely correlated to fat mass in males ($R = 0.26$, $p < 2e-13$) and females ($R = -0.4$, $p < 2e-16$).

(D) Percent area stained for *UCP1* in intact and gonadectomized C57BL/6J mice fed chow and HF/HS diets. The x axis labels refer to histological panels in (E)–(L).

(E–L) Representative *UCP1* staining from gonadal fat of mice. Coding of sex, diet, and GDX as in (D).

(legend continued on next page)

traits in both males and females. Surprisingly, the correlations were in the opposite direction in the two sexes (Figures 6B, 6C, and S5). Specifically in females, increased *Ucp1* expression was correlated with better metabolic profiles, whereas in males, the expression of *Ucp1* seemed to reflect poorer response to HF diet, increased insulin resistance, and larger fat mass accumulation (Figures 6B and 6C). Moreover, while in females, *Ucp1* expression was significantly correlated with other key genes in the browning process, such as the transcription factor *Ppargc1a*, these correlations were not observed in males (Figure S6). *Ucp1* did not exhibit a significant local eQTL, and therefore the genetic variation in transcript levels is regulated in *trans*.

Based on the above evidence, we have examined adipose tissue morphology, evidence for browning, and the extent to which these differences are regulated by sex hormones and diet in sham-operated and gonadectomized C57BL/6J mice (Figures 6D–6L). First, we extended our initial findings that *Ucp1* is more highly expressed in female gonadal fat (Figures 6A and S6) to the protein level (Figure 6D). Our results suggested that both HF/HS diet and sex hormones regulate *Ucp1* levels in the females (Figure 6D), while almost no *Ucp1* staining was detected in the males (with the exception of one sample in the gonadectomized chow group; Figure 6G). The effect of gonadectomy on *Ucp1* in females was confirmed using mRNA levels, although the fold-change was much smaller than that observed using protein staining of adipose (Figure S3B).

Next, we investigated if the ratio of large to small adipocytes was affected by gonadectomy in C57BL/6J, C3H/HeJ, and DBA/2J mice fed either a chow or an HF/HS diet. Whereas no effects of gonadectomy were observed in male mice fed either diet, gonadectomy increased the number of large adipocytes in female mice fed a chow diet (Figure 6M). The effect of gonadectomy on adipocytes reached significance in C3H/HeJ and DBA/2J. No effect of gonadectomy was observed on the ratio of large to small adipocytes in female mice fed an HF/HS diet. These data suggest that a sex hormone-by-diet effect exists in females and that the protective effect of female sex hormones on adipocyte size is ablated by an unhealthy diet.

Gene-by-Sex Interactions Affecting Isolated Mitochondria

We evaluated mitochondrial number and function in male and female mice from three different inbred strains fed a chow diet: A/J, C57BL/6J, and C3H/HeJ (Figure 7). First, we measured the amount of mitochondrial DNA (Figure 7A). In A/J and C3H/HeJ, but not C57BL/6J mice, females showed higher content of mitochondrial DNA than males. Next, we investigated whether we could find a sex difference in mitochondrial respiration after normalization to mitochondrial content. We isolated mitochondria from white adipose tissues (gonadal and inguinal) and measured respiration of specific mitochondrial respiratory chain complexes. In A/J and C3H/HeJ mice, respiration from gonadal adipose mitochondria was higher in female than male mice in all complexes (Figures 7B and 7C), with respiratory chain com-

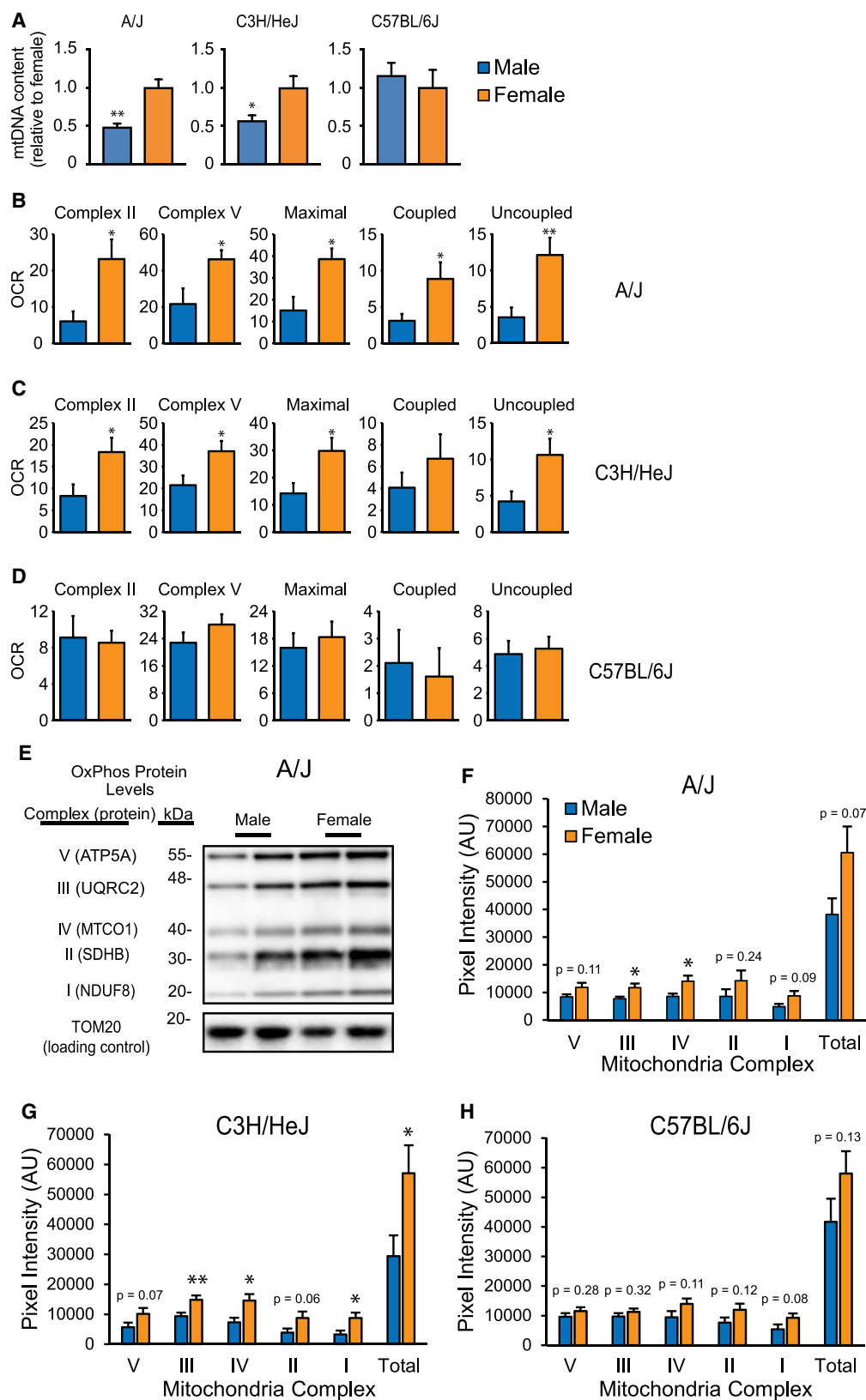
plexes II and V as well as maximal respiration rates showing around a 2-fold difference. The increase in respiration in females was due to both coupled and uncoupled respiration. In contrast, no significant differences were observed in the commonly used strain C57BL/6J (Figure 7D). Similar results were obtained with inguinal mitochondria (data not shown). To examine whether this sex difference was dependent on diet, we repeated the study on gonadal adipose tissue from A/J and C57BL/6J mice after 8 weeks of HF/HS feeding (Figure S7). Similar to our chow-fed mice, we found increased mitochondrial respiration in females as compared to males in A/J mice (Figure S7A). In contrast, we observed a significant increase only in the uncoupled respiration in C57BL/6J females as compared to their male counterparts when fed an HF/HS diet (Figure S7B). Though *Ucp1* expression is higher in C57BL/6J females under both dietary conditions, we believe that external stimuli such as excess caloric intake during HF/HS treatment or additional modifiers may be needed to functionally activate UCP1-mediated uncoupled respiration in C57BL/6J females. However, this was not required for A/J and C3H/HeJ. Consistent with changes in mitochondrial respiration, female A/J and C3H/HeJ mice showed enhanced protein content of several mitochondrial electron transport chain complexes as compared to males (Figures 7E–7G). C57BL/6J mice also showed a tendency for increased protein content of several mitochondrial electron transport chain complexes in females as compared to males, but these differences did not reach significance (Figure 7H). These results demonstrate a gene-by-sex interaction affecting mitochondrial function in mice. Notably, when challenged with an HF/HS diet, A/J was the most resistant to weight gain, C57BL/6J the most susceptible, and C3H/HeJ intermediate (Parks et al., 2013).

DISCUSSION

We report a comprehensive study of gene-by-sex differences in cardio-metabolic traits in a panel of about 100 genetically diverse inbred strains. Several conclusions have emerged from these studies. First, we observed prevalent gene-by-sex interactions in the cardio-metabolic traits studied and in regulation of gene expression in adipose and liver. Second, we obtained significant evidence for sex-specific GWAS for cardio-metabolic traits in mice, and we validated a sex-specific gene for diet-induced obesity, *Lypla1*. Third, we used transcriptional profiling of liver and adipose to explore the basic functions affected by sex in those tissues and found that sex affects regulation of gene expression in a tissue-specific manner with strong genetic interactions. Notably, gonadectomy studies indicated that the gene expression differences between sexes in liver but not adipose were largely because of reversible hormonal effects. The gene expression studies strongly pointed to an important role of adipose mitochondria in the sex differences. This was confirmed using immunohistochemistry of adipose and functional analyses of isolated mitochondria. Each of these points is discussed in turn below.

(M) Percent of large adipocytes (large/total number of adipocytes) in intact and gonadectomized C57BL/6J, C3H/HeJ, and DBA/2J mice fed chow or HF/HS diet.

* $p < 0.05$ and ** $p < 0.01$ between gonadectomized group (GDX) and sham-operated controls. p values were calculated using a Student's t test (two-way).



(legend on next page)

The cardio-metabolic traits studied here exhibit striking sex-specific interdependencies, as evidenced both by trait-trait correlations and by the specificity of trait-transcript correlations. This is consistent with results of some previous studies (Traglia et al., 2017) and suggests the existence of common sex-specific higher-order interactions rather than pathways that perturb individual traits. Gene expression is an important mediator of sex-specific effects and of common genetic variation, but our understanding of how gene-by-sex interactions modulate gene expression variability is limited at best. Our findings emphasize the high degree of tissue specificity for sex effects on expression. This manifests in almost complete independence of sex effects on gene expression in adipose and liver and in tissue specificity of gene-by-sex eQTLs. Notably, we find that ~80% of eQTLs that are shared between tissues are also shared between sexes, whereas only ~50% of tissue-specific eQTLs are shared between males and females. Concurrently, we also show that hormones have tissue-specific effects on transcriptome measures. Together, these results suggest profound differences between male and female tissues at the very basic, cellular function as well as tissue composition.

Very few studies addressing gene-by-sex interactions at the level of cardio-metabolic phenotypes have been reported (Andreux et al., 2012; Dimas et al., 2012; Liu et al., 2012a; Myers et al., 2014; Rawlik et al., 2016). In general, sex differences in the genetic architecture of human disease (Afshari et al., 2017; Chen et al., 2018; Kwon et al., 2017; Lu et al., 2017) and anthropometric traits (Karp et al., 2017; Kukurba et al., 2016; Nookaew et al., 2013; Palmer and Clegg, 2014; Randall et al., 2013; Weiss et al., 2006; White and Tchoukalova, 2014) are suggested by some studies, yet others failed to find evidence for prevalent sex-specific genetic associations in mouse and human (Krohn et al., 2014). Our results clearly indicate that gene-by-sex interactions are common in mice, at least for metabolic traits. The importance of gene-by-sex interactions is further supported by the finding that GWAS loci in mice frequently exhibit sex-specific effects. This finding contrasts with GWAS results in human studies, where few instances of sex-specific loci have been reported (<http://www.ebi.ac.uk/gwas/>) (Liu et al., 2012b; Randall et al., 2013). The explanation for this discrepancy is unclear and likely arises from more than one reason. It may be that sex differences are more pronounced and prevalent in mice, in which case mapping of traits in a sex-specific manner increases the power to map loci in mice. Another possibility is that among the mouse loci there are false positives, which in turn contribute to the sex specificity. However, sex-specific QTLs have also been noted for metabolic and other traits using traditional intercrosses in mice (Melo et al., 1996; Wang et al., 2006). Another likely contributing factor is that human GWAS analyses are rarely reported separately for males and females, where sex

is frequently used as a factor in linear regression model rather than in separate analysis. The validity of such approach depends on the actual difference between sexes relative to sample size, but in general, this inherently reduces the power to identify sex-specific QTLs. As shown here for mice, gene-by-sex interactions are prevalent, and the use of regression models is likely to obscure both the effects of sex and genetics. In general, human GWAS identify modest effects, and the sample sizes required to have a robust mapping are in the tens to hundreds of thousands. Dividing that sample into two separate groups will often result in an unacceptable reduction in power, even if the proportion of each sex in these groups is roughly 50%.

We examined one sex-specific GWAS locus for adiposity in detail and identified *Lyplal1* as the underlying gene. *Lyplal1* deficiency in female mice significantly increased BF% growth during the first 2 weeks of the HF/HS diet, indicating that *Lyplal1* protects against fat mass gain after switching to a diet rich in refined sugar and fat. This effect was not observed in male mice, suggesting that the observed gene-by-diet effect of *Lyplal1* is specific for females. It is unclear whether the missense variant, the *cis*-eQTL, or both are driving the sex-specific effect on body fat gain in response to the HF/HS diet. The fact that the heterozygous *Lyplal1* KO mice are very similar to the WT mice suggests that the effect is not dose dependent. This would be consistent with the scenario in which a strongly damaging missense variant is responsible. A likely mechanism explaining the sex-specific locus is that the function of *Lyplal1* is more important in females than males. This is not only supported by the sex-specific GWAS mapping but also by the fact that *Lyplal1* is more highly expressed in female mice. The magnitude of the change we observed in the KO experiment was approximately half of the allelic effect seen in the hfHMDP. A likely explanation for this is that there are interactions between the differing genetic backgrounds of the inbred mice and the genetic variation at the rs31134248 locus. It is also possible that we would observe a larger effect of knocking-out *Lyplal1* in one of the female strains with higher *Lyplal1* expression because female strain C57BL/6J mice exhibit relatively low *Lyplal1* expression compared to most hfHMDP mice. Several human GWAS studies have identified SNPs close to *Lyplal1* that associate with waist-to-hip ratio in women, but not men (Heid et al., 2010; Lindgren et al., 2009; Randall et al., 2013). In addition, Fox et al. (2012) showed that a SNP close to *Lyplal1* is associated with visceral to subcutaneous adipose tissue ratio in women. A recent study found no significant effect of *Lyplal1* deficiency on adiposity in mice (Watson et al., 2017). However, in accordance with our data, they found a tendency for increased adiposity in the female but not in male, *Lyplal1* KO mice. The discrepancy between the data might be explained by the number of mice included (our study included more mice) in the study or a difference in diets used.

Figure 7. Gene-by-Sex Interactions in Mitochondrial Oxidation Functions

(A) Mitochondrial DNA content were measured in gonadal adipose of A/J, C3H/HeJ, and C57BL/6J mice of both sexes.
(B–D) Mitochondria were isolated from gonadal adipose of strains A/J (n = 5 for males and n = 8 for females), C3H/HeJ (n = 8 for both sexes), and C57BL/6J (n = 8 for both sexes) and oxidative functions tested using a Seahorse bioanalyzer. Different mitochondrial states were measured as described in STAR Methods. Oxygen consumption rate (OCR) was normalized to μg mitochondrial protein (pmol/min/ μg protein).
(E–H) Representative immunoblot for A/J (E) and corresponding quantification for A/J (F), C3H/HeJ (G), and C57BL/6J (H) of electron transport chain components in adipose mitochondria. Mitochondrial contents were normalized to cellular protein contents for quantification, and TOM20 is shown as a loading control. Results are presented as mean \pm SEM. *p < 0.05 and **p < 0.01 between the sexes. p values were calculated using a Student's t test (two-way).

We examined the basis of the sex-dependent differences in gene expression. Tissue specificity of eQTLs is well documented, and results from a GTEx consortium that compared eQTLs identified in >40 human tissues suggests that up to 20%–50% of local eQTLs are tissue specific. However, very few studies have addressed the sex specificity of eQTLs. A recent study in human blood monocytes focused on chromosome X variants only (Castagné et al., 2011), while mouse eQTL studies either examined this question in a limited subset of genes or in intercrosses of only two strains (Yang et al., 2006). Our data suggest that while thousands of genes are differentially regulated between males and females in each tissue, only a small proportion of these differences are due to local gene-by-sex interactions. This is similar to results from some human studies (Dimas et al., 2012; Trabzuni et al., 2013; Yao et al., 2014). Therefore, it appears that the sex-specific differences in gene expression that are influenced by genetic background are regulated largely in *trans*. This is consistent with our findings discussed above that the basis of sex differences involve higher-order interactions, such as alterations of mitochondrial functions. Our data also show that gonadal hormones play a major role in modulating gene expression in metabolic tissues, but their effects in each tissue are distinct. Genes encoded by the X and Y chromosomes showed common patterns of sex-specific regulation in the two tissues, probably because of shared patterns of sex bias caused by escape from X inactivation (leading to higher expression in XX than XY cells) and male-specific expression of Y genes involved in basic cellular functions (Arnold, 2017; Bellott et al., 2014). Otherwise; however, the pattern of sex-specific regulation in the two tissues was almost entirely different. When we used total transcriptome for PCA of gene expression (Figure 5), it was evident that sex and diet represent the first 2 PCs in intact mice, accounting for more than 70% of the variability in gene expression. PCA with gonadectomized mice showed that in liver, the removal of male gonadal hormones resulted in a dramatic shift of male expression such that they resembled those in females, while gonadectomy had only a modest effect on gene expression in females. Notably, in liver, the effect was almost completely aligned with the sex principal component (PC1), suggesting that diet (represented by PC2) and gonadal hormones generally exert independent effects on liver gene expression. Strikingly, in the adipose, the pattern of gene expression was only modestly affected by gonadectomy in both males and females, and the direction of the shift was not along the male-female axis. These results suggest that male gonadal hormones (presumably testosterone) are critical for continuous sex-specific regulation in liver and that the sex differences in adipose might result more from organizational hormonal effect (developmental and permanent) or sex chromosome effects (Arnold, 2017).

We have followed up the global expression differences by examining adipose metabolism in more detail. We observed significant differences in the size of adipocytes, with females generally exhibiting smaller adipocytes on both chow and HF diets. This difference was partly eliminated by gonadectomy supporting a role of gonadal hormones. The gene expression analyses supported a role of mitochondria in the sex differences and, in particular, we observed that *Ucp1* was expressed more highly in female adipose. We confirmed this difference using

immunohistochemical staining. To determine whether there were functional differences, we isolated mitochondria from three strains with highly divergent sex differences, C57BL/6J, C3H/HeJ, and A/J. We observed particularly striking differences in mitochondrial functions in C3H/HeJ and A/J, where the oxygen consumption in females was approximately twice of that in males (Figures 7B and 7C). Notably, the difference was considerably reduced or absent in the commonly used strain C57BL/6J, providing a striking example of a gene-by-sex interaction at the molecular level (Figure 7D). Corresponding differences in the electron transport chain components were also observed in A/J, C3H/HeJ, and C57BL/6J mice (Figures 7E–7H). Many studies, primarily of strain C57BL/6J, have shown that females are more resistant to diet-induced obesity and measures of insulin resistance (Karp et al., 2017; Lovejoy et al., 2009; Parks et al., 2015; Varlamov et al., 2014; Yang et al., 2006), but the mechanisms involved have been unclear. In studies across the HMDP strains, we have observed that this is not a strain-specific finding for insulin resistance, although for certain strains, females are more susceptible to diet-induced obesity (Figure 2). In our analyses of strain C57BL/6J mice fed an HF diet, we observed higher uncoupled respiration in females compared to males, which may partly explain this resistance (Figure S7). Previously, it has been reported that HF diet feeding increased gonadal fat depot weight by adipocyte hypertrophy and hyperplasia in females but hypertrophy alone in male mice (Wu et al., 2017). Furthermore, estrogens protected female mice that underwent ovariectomy from adipocyte hypertrophy and from developing adipose tissue oxidative stress and inflammation (Stubbins et al., 2012). Our findings are in line with reports of a metabolically more active gonadal white adipose tissue of female mice compared to male mice that was characterized by enhanced lipolysis and recruitment of brown adipocytes (Dobner et al., 2017; Kim et al., 2016). Moreover, there is growing evidence for a role of mitochondria in pathologies with sex differences (Silkaitis and Lemos, 2014; Ventura-Clapier et al., 2017). Given that the expression of *Ucp1* and other markers of gene mitochondrial function are strongly correlated with metabolic health parameters, it is likely that mitochondrial function in adipose tissue is a major factor that underlies the sex differences.

Our results have raised a number of questions. Are sex-specific differences well conserved between species? In particular, do the differences in adipose mitochondrial function also occur in humans? It is clear that major differences exist in adipose biology between sexes in humans (Karastergiou et al., 2013). A study of 732 members of 154 nuclear families found that adipose resting energy expenditure was significantly higher in women than men. These authors then examined gene expression in subcutaneous adipose in a separate cohort as well as a subset of their cohort and observed higher expression of genes involved in mitochondrial function, including UCP1, in women than men, similar to our findings in mice (Nookaew et al., 2013). How do liver and adipose differ in epigenetic organization in sexual development (Ghahramani et al., 2014; McCarthy et al., 2017), and when do these organizational changes occur in development? Also, are cardio-metabolic traits unusual in the degree of sex-dependent effects? While our work adds insight into the depth and breadth of sex differences in metabolism, it also emphasizes the relative lack of understanding of the biology

underlying these differences. Previously, we have proposed as a long-term goal the development of a biologic network model that describes the differences between males and females (the “sex-ome”) on a system level (Arnold and Lusis, 2012). Such a model will require identifying the primary and downstream sex-biased factors that act on the network and how the sex-biased network interactions give rise to sex differences in the emergent phenotypes. We believe that our results provide compelling evidence as to why males and females in biological research should be treated as distinct organisms as a whole, rather than attempting to reconcile these differences one molecule at a time.

Limitations of Study

Our study has several limitations. The mechanistic studies were limited to liver and adipose, and the role of estrogen was not explored. Although some evidence, discussed above, suggests that humans exhibit sexual dimorphisms for mitochondrial function, we did not directly test this.

STAR★METHODS

Detailed methods are provided in the online version of this paper and include the following:

- KEY RESOURCES TABLE
- CONTACT FOR REAGENT AND RESOURCE SHARING
- EXPERIMENTAL MODEL AND SUBJECT DETAILS
 - Animals
- METHOD DETAILS
 - Phenotype-Phenotype Correlations
 - RNA Library Preparation and Sequencing
 - Tissue Deconvolution
 - Heritability
 - Genome-Wide Association Analyses
 - *Lyplal1* Studies
 - Mitochondrial DNA Content
 - Mitochondrial Bioenergetics
 - Mitochondrial Immunoblot Procedures and Analyses of Function
 - Immunohistochemistry
- QUANTIFICATION AND STATISTICAL ANALYSIS
 - Statistical Analyses
- DATA AND SOFTWARE AVAILABILITY

SUPPLEMENTAL INFORMATION

Supplemental Information includes seven figures and four tables and can be found with this article online at <https://doi.org/10.1016/j.cmet.2018.12.013>.

ACKNOWLEDGMENTS

We thank Rosa Chen for help in preparing the manuscript, Sarada Charugundla for plasma metabolite analysis, and Yonghong Meng for immunoblot analysis. We also thank Sebastian Cucuruz and Cynthia Striese from the Helmholtz Center for scanning the UCP-1 and Caspase 3 immuno-staining. This work was supported by the NIH grants HL28481, HL30568, K99-HL138193, T32-HL69766, T32-HL007895, and R00-HL123021; Transatlantic Network of Excellence Award 12CVD02; The Research Council of Norway (240405/F20); the Helmholtz Alliance ICEMED (Imaging and Curing Environmental Metabolic Diseases); the Network Fund of the Helmholtz Association; the German Center for Diabetes Research (DZD); the American Heart Association (AHA) fellowship

18POST33990256; and Project A4 (principal investigator S.M.H.) of the SFB1123 from the German Research Foundation (DFG).

AUTHOR CONTRIBUTIONS

F.N., Y.H.-B., K.C.K., M.M.S., and A.J.L. designed all the experiments. F.N., Y.H.-B., L.V., K.C.K., M.M.S., S.T.H., M.M., Z.Z., S.G., B.W.P., and A.W. performed the experiments. F.N., Y.H.-B., L.V., K.C.K., C.P., M.M.S., A.W., K.R., S.M.H., and A.J.L. analyzed raw data. F.N., Y.H.-B., K.C.K., M.M.S., A.P.A., and A.J.L. wrote the manuscript, which was reviewed by all authors.

DECLARATION OF INTERESTS

The authors declare no competing interests.

Received: April 23, 2018

Revised: August 29, 2018

Accepted: December 17, 2018

Published: January 10, 2019

REFERENCES

- Afshari, N.A., Igo, R.P., Jr., Morris, N.J., Stambolian, D., Sharma, S., Pulagam, V.L., Dunn, S., Stamler, J.F., Truitt, B.J., Rimmier, J., et al. (2017). Genome-wide association study identifies three novel loci in Fuchs endothelial corneal dystrophy. *Nat. Commun.* 8, 14898.
- Andreux, P.A., Williams, E.G., Koutnikova, H., Houtkooper, R.H., Champy, M.F., Henry, H., Schoonjans, K., Williams, R.W., and Auwerx, J. (2012). Systems genetics of metabolism: the use of the BXD murine reference panel for multiscale integration of traits. *Cell* 150, 1287–1299.
- Arnold, A.P. (2009). The organizational-activational hypothesis as the foundation for a unified theory of sexual differentiation of all mammalian tissues. *Horm. Behav.* 55, 570–578.
- Arnold, A.P. (2017). A general theory of sexual differentiation. *J. Neurosci. Res.* 95, 291–300.
- Arnold, A.P., and Lusis, A.J. (2012). Understanding the sexome: measuring and reporting sex differences in gene systems. *Endocrinology* 153, 2551–2555.
- Bellott, D.W., Hughes, J.F., Skaletsky, H., Brown, L.G., Pyntikova, T., Cho, T.J., Koutseva, N., Zaghlul, S., Graves, T., Rock, S., et al. (2014). Mammalian Y chromosomes retain widely expressed dosage-sensitive regulators. *Nature* 508, 494–499.
- Bennett, B.J., Farber, C.R., Orozco, L., Min Kang, H.M., Ghazalpour, A., Siemers, N., Neubauer, M., Neuhaus, I., Yordanova, R., Guan, B., et al. (2010). A high-resolution association mapping panel for the dissection of complex traits in mice. *Genome Res.* 20, 281–290.
- Bouret, S.G. (2013). Organizational actions of metabolic hormones. *Front. Neuroendocrinol.* 34, 18–26.
- Byers, S.L., Wiles, M.V., Dunn, S.L., and Taft, R.A. (2012). Mouse estrous cycle identification tool and images. *PLoS One* 7, e35538.
- Cannon, B., and Nedergaard, J. (2004). Brown adipose tissue: function and physiological significance. *Physiol. Rev.* 84, 277–359.
- Capel, B. (2017). Vertebrate sex determination: evolutionary plasticity of a fundamental switch. *Nat. Rev. Genet.* 18, 675–689.
- Castagné, R., Zeller, T., Rotival, M., Szymczak, S., Truong, V., Schillert, A., Trégouët, D.A., Münzel, T., Ziegler, A., Cambien, F., et al. (2011). Influence of sex and genetic variability on expression of X-linked genes in human monocytes. *Genomics* 98, 320–326.
- Charlesworth, B. (1996). The evolution of chromosomal sex determination and dosage compensation. *Curr. Biol.* 6, 149–162.
- Chen, H., Cade, B.E., Gleason, K.J., Bjonnes, A.C., Stip, A.M., Sofer, T., Conomos, M.P., Ancoli-Israel, S., Arens, R., Azarbarzin, A., et al. (2018). Multi-ethnic meta-analysis identifies RAI1 as a possible obstructive sleep apnea related quantitative trait locus in men. *Am. J. Respir. Cell Mol. Biol.* 58, 391–401.

- Chen, X., McClusky, R., Chen, J., Beaven, S.W., Tontonoz, P., Arnold, A.P., and Reue, K. (2012). The number of X chromosomes causes sex differences in adiposity in mice. *PLoS Genet.* 8, e1002709.
- Choi, Y., and Chan, A.P. (2015). PROVEAN web server: a tool to predict the functional effect of amino acid substitutions and indels. *Bioinformatics* 31, 2745–2747.
- Della Torre, S., Mitro, N., Meda, C., Lolli, F., Pedretti, S., Barcella, M., Ottobri, L., Metzger, D., Caruso, D., and Maggi, A. (2018). Short-term fasting reveals amino acid metabolism as a major sex-discriminating factor in the liver. *Cell Metab.* 28, 256–267.e5.
- Dimas, A.S., Nica, A.C., Montgomery, S.B., Stranger, B.E., Raj, T., Buil, A., Giger, T., Lappalainen, T., Gutierrez-Arcelus, M., McCarthy, M.I., et al. (2012). Sex-biased genetic effects on gene regulation in humans. *Genome Res.* 22, 2368–2375.
- Disteche, C.M. (2012). Dosage compensation of the sex chromosomes. *Annu. Rev. Genet.* 46, 537–560.
- Dobner, J., Ress, C., Rufinatscha, K., Salzmann, K., Salvenmoser, W., Folie, S., Wieser, V., Moser, P., Weiss, G., Goebel, G., et al. (2017). Fat-enriched rather than high-fructose diets promote whitening of adipose tissue in a sex-dependent manner. *J. Nutr. Biochem.* 49, 22–29.
- Falls, J.G., Ryu, D.Y., Cao, Y., Levi, P.E., and Hodgson, E. (1997). Regulation of mouse liver flavin-containing monooxygenases 1 and 3 by sex steroids. *Arch. Biochem. Biophys.* 342, 212–223.
- Fields, C.T., Chassaing, B., Paul, M.J., Gewirtz, A.T., and de Vries, G.J. (2017). Vasopressin deletion is associated with sex-specific shifts in the gut microbiome. *Gut Microbes* 9, 13–25.
- Fox, C.S., Liu, Y., White, C.C., Feitosa, M., Smith, A.V., Heard-Costa, N., Lohman, K., Johnson, A.D., Foster, M.C., Greenawalt, D.M., et al. (2012). Genome-wide association for abdominal subcutaneous and visceral adipose reveals a novel locus for visceral fat in women. *PLoS Genet.* 8, e1002695.
- Ghahramani, N.M., Ngun, T.C., Chen, P.Y., Tian, Y., Krishnan, S., Muir, S., Rubbi, L., Arnold, A.P., de Vries, G.J., Forger, N.G., et al. (2014). The effects of perinatal testosterone exposure on the DNA methylome of the mouse brain are late-emerging. *Biol. Sex Differ.* 5, 8.
- Giordano, A., Frontini, A., and Cinti, S. (2016). Convertible visceral fat as a therapeutic target to curb obesity. *Nat. Rev. Drug Discov.* 15, 405–424.
- Gregg, C., Zhang, J., Butler, J.E., Haig, D., and Dulac, C. (2010). Sex-specific parent-of-origin allelic expression in the mouse brain. *Science* 329, 682–685.
- Hager, R., Cheverud, J.M., Leamy, L.J., and Wolf, J.B. (2008). Sex dependent imprinting effects on complex traits in mice. *BMC Evol. Biol.* 8, 303.
- Hasin-Brumshtein, Y., Khan, A.H., Hormozdizadeh, F., Pan, C., Parks, B.W., Petyuk, V.A., Piehowski, P.D., Brümmer, A., Pellegrini, M., Xiao, X., et al. (2016). Hypothalamic transcriptomes of 99 mouse strains reveal trans eQTL hotspots, splicing QTLs and novel non-coding genes. *Elife* 5, e15614.
- Heid, I.M., Jackson, A.U., Randall, J.C., Winkler, T.W., Qi, L., Steinthorsdottir, V., Thorleifsson, G., Zillikens, M.C., Speliotes, E.K., Mägi, R., et al. (2010). Meta-analysis identifies 13 new loci associated with waist-hip ratio and reveals sexual dimorphism in the genetic basis of fat distribution. *Nat. Genet.* 42, 949–960.
- Jalouli, M., Carlsson, L., Améen, C., Lindén, D., Ljungberg, A., Michalik, L., Edén, S., Wahli, W., and Oscarsson, J. (2003). Sex difference in hepatic peroxisome proliferator-activated receptor alpha expression: influence of pituitary and gonadal hormones. *Endocrinology* 144, 101–109.
- Karastergiou, K., Fried, S.K., Xie, H., Lee, M.J., Divoux, A., Rosencrantz, M.A., Chang, R.J., and Smith, S.R. (2013). Distinct developmental signatures of human abdominal and gluteal subcutaneous adipose tissue depots. *J. Clin. Endocrinol. Metab.* 98, 362–371.
- Karp, N.A., Mason, J., Beaudet, A.L., Benjamini, Y., Bower, L., Braun, R.E., Brown, S.D.M., Chesler, E.J., Dickinson, M.E., Flenniken, A.M., et al. (2017). Prevalence of sexual dimorphism in mammalian phenotypic traits. *Nat. Commun.* 8, 15475.
- Kenney-Hunt, J.P., Wang, B., Norgard, E.A., Fawcett, G., Falk, D., Pletscher, L.S., Jarvis, J.P., Roseman, C., Wolf, J., and Cheverud, J.M. (2008). Pleiotropic patterns of quantitative trait loci for 70 murine skeletal traits. *Genetics* 178, 2275–2288.
- Kim, S.N., Jung, Y.S., Kwon, H.J., Seong, J.K., Granneman, J.G., and Lee, Y.H. (2016). Sex differences in sympathetic innervation and browning of white adipose tissue of mice. *Biol. Sex Differ.* 7, 67.
- Krohn, J., Speed, D., Palme, R., Touma, C., Mott, R., and Flint, J. (2014). Genetic interactions with sex make a relatively small contribution to the heritability of complex traits in mice. *PLoS One* 9, e96450.
- Kukurba, K.R., Parsana, P., Balliu, B., Smith, K.S., Zappala, Z., Knowles, D.A., Favé, M.J., Davis, J.R., Li, X., Zhu, X., et al. (2016). Impact of the X chromosome and sex on regulatory variation. *Genome Res.* 26, 768–777.
- Kwekel, J.C., Vijay, V., Han, T., Moland, C.L., Desai, V.G., and Fuscoe, J.C. (2017). Sex and age differences in the expression of liver microRNAs during the life span of F344 rats. *Biol. Sex Differ.* 8, 6.
- Kwon, Y.C., Kim, J.J., Yun, S.W., Yu, J.J., Yoon, K.L., Lee, K.Y., Kil, H.R., Kim, G.B., Han, M.K., Song, M.S., et al. (2017). Male-specific association of the FCGR2A His167Arg polymorphism with Kawasaki disease. *PLoS One* 12, e0184248.
- Lindgren, C.M., Heid, I.M., Randall, J.C., Lamina, C., Steinthorsdottir, V., Qi, L., Speliotes, E.K., Thorleifsson, G., Willer, C.J., Herrera, B.M., et al. (2009). Genome-wide association scan meta-analysis identifies three loci influencing adiposity and fat distribution. *PLoS Genet.* 5, e1000508.
- Link, J.C., Chen, X., Arnold, A.P., and Reue, K. (2013). Metabolic impact of sex chromosomes. *Adipocyte* 2, 74–79.
- Link, J.C., and Reue, K. (2017). Genetic basis for sex differences in obesity and lipid metabolism. *Annu. Rev. Nutr.* 37, 225–245.
- Liu, C.T., Estrada, K., Yerges-Armstrong, L.M., Amin, N., Evangelou, E., Li, G., Minster, R.L., Carless, M.A., Kammerer, C.M., Oei, L., et al. (2012a). Assessment of gene-by-sex interaction effect on bone mineral density. *J. Bone Miner. Res.* 27, 2051–2064.
- Liu, L.Y., Schaub, M.A., Sirota, M., and Butte, A.J. (2012b). Sex differences in disease risk from reported genome-wide association study findings. *Hum. Genet.* 131, 353–364.
- Lovejoy, J.C., and Sainsbury, A.; Stock Conference 2008 Working Group (2009). Sex differences in obesity and the regulation of energy homeostasis. *Obes. Rev.* 10, 154–167.
- Lu, S., Zhao, L.J., Chen, X.D., Pappasian, C.J., Wu, K.H., Tan, L.J., Wang, Z.E., Pei, Y.F., Tian, Q., and Deng, H.W. (2017). Bivariate genome-wide association analyses identified genetic pleiotropic effects for bone mineral density and alcohol drinking in Caucasians. *J. Bone Miner. Metab.* 35, 649–658.
- Lusis, A.J., Seldin, M.M., Allayee, H., Bennett, B.J., Civelek, M., Davis, R.C., Eskin, E., Farber, C.R., Hui, S., Mehrabian, M., et al. (2016). The Hybrid Mouse Diversity Panel: a resource for systems genetics analyses of metabolic and cardiovascular traits. *J. Lipid Res.* 57, 925–942.
- McCarthy, M.M., Auger, A.P., Bale, T.L., De Vries, G.J., Dunn, G.A., Forger, N.G., Murray, E.K., Nugent, B.M., Schwarz, J.M., and Wilson, M.E. (2009). The epigenetics of sex differences in the brain. *J. Neurosci.* 29, 12815–12823.
- McCarthy, M.M., Nugent, B.M., and Lenz, K.M. (2017). Neuroimmunology and neuroepigenetics in the establishment of sex differences in the brain. *Nat. Rev. Neurosci.* 18, 471–484.
- Melo, J.A., Shendure, J., Pociask, K., and Silver, L.M. (1996). Identification of sex-specific quantitative trait loci controlling alcohol preference in C57BL/6 mice. *Nat. Genet.* 13, 147–153.
- Mittelstrass, K., Ried, J.S., Yu, Z., Krumsiek, J., Gieger, C., Prehn, C., Roemisch-Margl, W., Polonikov, A., Peters, A., Theis, F.J., et al. (2011). Discovery of sexual dimorphisms in metabolic and genetic biomarkers. *PLoS Genet.* 7, e1002215.
- Mozhui, K., Lu, L., Armstrong, W.E., and Williams, R.W. (2012). Sex-specific modulation of gene expression networks in murine hypothalamus. *Front. Neurosci.* 6, 63.
- Myers, R.A., Scott, N.M., Gauderman, W.J., Qiu, W., Mathias, R.A., Romieu, I., Levin, A.M., Pino-Yanes, M., Graves, P.E., Villarréal, A.B., et al. (2014). Genome-wide interaction studies reveal sex-specific asthma risk alleles. *Hum. Mol. Genet.* 23, 5251–5259.

- Nookaew, I., Svensson, P.A., Jacobson, P., Jernås, M., Taube, M., Larsson, I., Andersson-Assarsson, J.C., Sjöström, L., Froguel, P., Walley, A., et al. (2013). Adipose tissue resting energy expenditure and expression of genes involved in mitochondrial function are higher in women than in men. *J. Clin. Endocrinol. Metab.* **98**, E370–E378.
- Ober, C., Loisel, D.A., and Gilad, Y. (2008). Sex-specific genetic architecture of human disease. *Nat. Rev. Genet.* **9**, 911–922.
- Org, E., Mehrabian, M., Parks, B.W., Shipkova, P., Liu, X., Drake, T.A., and Lusis, A.J. (2016). Sex differences and hormonal effects on gut microbiota composition in mice. *Gut Microbes* **7**, 313–322.
- Orozco, L.D., Bennett, B.J., Farber, C.R., Ghazalpour, A., Pan, C., Che, N., Wen, P., Qi, H.X., Mutukulu, A., Siemers, N., et al. (2012). Unraveling inflammatory responses using systems genetics and gene-environment interactions in macrophages. *Cell* **151**, 658–670.
- Palmer, B.F., and Clegg, D.J. (2014). Oxygen sensing and metabolic homeostasis. *Mol. Cell. Endocrinol.* **397**, 51–58.
- Parks, B.W., Nam, E., Org, E., Kostem, E., Norheim, F., Hui, S.T., Pan, C., Civelek, M., Rau, C.D., Bennett, B.J., et al. (2013). Genetic control of obesity and gut microbiota composition in response to high-fat, high-sucrose diet in mice. *Cell Metab.* **17**, 141–152.
- Parks, B.W., Sallam, T., Mehrabian, M., Psychogios, N., Hui, S.T., Norheim, F., Castellani, L.W., Rau, C.D., Pan, C., Phun, J., et al. (2015). Genetic architecture of insulin resistance in the mouse. *Cell Metab.* **21**, 334–347.
- Randall, J.C., Winkler, T.W., Kutalik, Z., Berndt, S.I., Jackson, A.U., Monda, K.L., Kilpeläinen, T.O., Esko, T., Mägi, R., Li, S., et al. (2013). Sex-stratified genome-wide association studies including 270,000 individuals show sexual dimorphism in genetic loci for anthropometric traits. *PLoS Genet.* **9**, e1003500.
- Rau, C.D., Parks, B., Wang, Y., Eskin, E., Simecek, P., Churchill, G.A., and Lusis, A.J. (2015). High-density genotypes of inbred mouse strains: improved power and precision of association mapping. *G3 (Bethesda)* **5**, 2021–2026.
- Rawlik, K., Canela-Xandri, O., and Tenesa, A. (2016). Evidence for sex-specific genetic architectures across a spectrum of human complex traits. *Genome Biol.* **17**, 166.
- Rinn, J.L., Rozowsky, J.S., Laurenzi, I.J., Petersen, P.H., Zou, K., Zhong, W., Gerstein, M., and Snyder, M. (2004). Major molecular differences between mammalian sexes are involved in drug metabolism and renal function. *Dev. Cell* **6**, 791–800.
- Rinn, J.L., and Snyder, M. (2005). Sexual dimorphism in mammalian gene expression. *Trends Genet.* **21**, 298–305.
- Rooney, J.P., Ryde, I.T., Sanders, L.H., Howlett, E.H., Colton, M.D., Germ, K.E., Mayer, G.D., Greenamyre, J.T., and Meyer, J.N. (2015). PCR based determination of mitochondrial DNA copy number in multiple species. *Methods Mol. Biol.* **1241**, 23–38.
- Roy, A.K., and Chatterjee, B. (1983). Sexual dimorphism in the liver. *Annu. Rev. Physiol.* **45**, 37–50.
- Seldin, M.M., Kim, E.D., Romay, M.C., Li, S., Rau, C.D., Wang, J.J., Krishnan, K.C., Wang, Y., Deb, A., and Lusis, A.J. (2017). A systems genetics approach identifies Trp53inp2 as a link between cardiomyocyte glucose utilization and hypertrophic response. *Am. J. Physiol. Heart Circ. Physiol.* **312**, H728–H741.
- Silkaitis, K., and Lemos, B. (2014). Sex-biased chromatin and regulatory cross-talk between sex chromosomes, autosomes, and mitochondria. *Biol. Sex Differ.* **5**, 2.
- Stubbins, R.E., Najjar, K., Holcomb, V.B., Hong, J., and Núñez, N.P. (2012). Oestrogen alters adipocyte biology and protects female mice from adipocyte inflammation and insulin resistance. *Diabetes Obes. Metab.* **14**, 58–66.
- Tai, E.S., Bin Ali, A., Zhang, Q., Loh, L.M., Tan, C.E., Retnam, L., El Oakley, R.M., and Lim, S.K. (2003). Hepatic expression of PPAR α , a molecular target of fibrates, is regulated during inflammation in a gender-specific manner. *FEBS Lett.* **546**, 237–240.
- Trabzuni, D., Ramasamy, A., Imran, S., Walker, R., Smith, C., Weale, M.E., Hardy, J., and Ryten, M.; North American Brain Expression (2013). Widespread sex differences in gene expression and splicing in the adult human brain. *Nat. Commun.* **4**, 2771.
- Traglia, M., Bseiso, D., Gusev, A., Adviento, B., Park, D.S., Mefford, J.A., Zaitlen, N., and Weiss, L.A. (2017). Genetic mechanisms leading to sex differences across common diseases and anthropometric traits. *Genetics* **205**, 979–992.
- van Nas, A., Guhathakurta, D., Wang, S.S., Yehya, N., Horvath, S., Zhang, B., Ingram-Drake, L., Chaudhuri, G., Schadt, E.E., Drake, T.A., et al. (2009). Elucidating the role of gonadal hormones in sexually dimorphic gene co-expression networks. *Endocrinology* **150**, 1235–1249.
- Varlamov, O., Bethea, C.L., and Roberts, C.T., Jr. (2014). Sex-specific differences in lipid and glucose metabolism. *Front. Endocrinol.* **5**, 241.
- Venegas, V., and Halberg, M.C. (2012). Methods in molecular biology. *Methods Mol. Biol. Clifton N.J.* **837**, 327–335.
- Ventura-Clapier, R., Moulin, M., Piquereau, J., Lemaire, C., Mericskay, M., Veksler, V., and Garnier, A. (2017). Mitochondria: a central target for sex differences in pathologies. *Clin. Sci.* **131**, 803–822.
- Vergnes, L., Chin, R., Young, S.G., and Reue, K. (2011). Heart-type fatty acid-binding protein is essential for efficient brown adipose tissue fatty acid oxidation and cold tolerance. *J. Biol. Chem.* **286**, 380–390.
- Vergnes, L., Davies, G.R., Lin, J.Y., Yeh, M.W., Livhits, M.J., Harari, A., Symonds, M.E., Sacks, H.S., and Reue, K. (2016). Adipocyte browning and higher mitochondrial function in perirenal but not SC fat in pheochromocytoma. *J. Clin. Endocrinol. Metab.* **101**, 4440–4448.
- Vieira Potter, V.J., Strissel, K.J., Xie, C., Chang, E., Bennett, G., Defuria, J., Obin, M.S., and Greenberg, A.S. (2012). Adipose tissue inflammation and reduced insulin sensitivity in ovariectomized mice occurs in the absence of increased adiposity. *Endocrinology* **153**, 4266–4277.
- Wang, S., Yehya, N., Schadt, E.E., Wang, H., Drake, T.A., and Lusis, A.J. (2006). Genetic and genomic analysis of a fat mass trait with complex inheritance reveals marked sex specificity. *PLoS Genet.* **2**, e15.
- Watson, R.A., Gates, A.S., Wynn, E.H., Calvert, F.E., Girousse, A., Lelliott, C.J., and Barroso, I. (2017). Lyplal1 is dispensable for normal fat deposition in mice. *Dis. Model. Mech.* **10**, 1481–1488.
- Weiss, L.A., Pan, L., Abney, M., and Ober, C. (2006). The sex-specific genetic architecture of quantitative traits in humans. *Nat. Genet.* **38**, 218–222.
- White, U.A., and Tchoukalova, Y.D. (2014). Sex dimorphism and depot differences in adipose tissue function. *Biochim. Biophys. Acta* **1842**, 377–392.
- Wu, Y., Lee, M.J., Ido, Y., and Fried, S.K. (2017). High-fat diet-induced obesity regulates MMP3 to modulate depot- and sex-dependent adipose expansion in C57BL/6J mice. *Am. J. Physiol. Endocrinol. Metab.* **312**, E58–E71.
- Yang, H., Ding, Y., Hutchins, L.N., Szatkiewicz, J., Bell, T.A., Paigen, B.J., Graber, J.H., de Villena, F.P., and Churchill, G.A. (2009). A customized and versatile high-density genotyping array for the mouse. *Nat. Methods* **6**, 663–666.
- Yang, J., Lee, S.H., Goddard, M.E., and Visscher, P.M. (2011). GCTA: a tool for genome-wide complex trait analysis. *Am. J. Hum. Genet.* **88**, 76–82.
- Yang, X., Schadt, E.E., Wang, S., Wang, H., Arnold, A.P., Ingram-Drake, L., Drake, T.A., and Lusis, A.J. (2006). Tissue-specific expression and regulation of sexually dimorphic genes in mice. *Genome Res.* **16**, 995–1004.
- Yao, C., Joeheanes, R., Johnson, A.D., Huan, T., Esko, T., Ying, S., Freedman, J.E., Murabito, J., Lunetta, K.L., Metspalu, A., et al. (2014). Sex- and age-interacting eQTLs in human complex diseases. *Hum. Mol. Genet.* **23**, 1947–1956.

STAR★METHODS

KEY RESOURCES TABLE

REAGENT or RESOURCE	SOURCE	IDENTIFIER
Antibodies		
Total OxPhos complex cocktail	Abcam	Cat# ab110413; RRID: AB_2629281
TOM20	Santa Cruz	Cat# sc-17764; RRID: AB_628381
UCP1	Abcam	Cat# ab10983; RRID: AB_2241462
Chemicals, Peptides, and Recombinant Proteins		
QIAzol Lysis Reagent	Qiagen	Cat# 79306
Chloroform, HPLC grade	Thermo Fisher	Cat# C606-4
Isopropanol, 99.5%, for molecular biology	Acros Organics	Cat# 32727-0010
Critical Commercial Assays		
High-Capacity cDNA Reverse Transcription Kit	Thermo Fisher	Cat# 4368813
KAPA SYBR FAST for LightCycler 480	KAPA Biosystems	Cat# 07959494001
Deposited Data		
HMDP expression arrays (liver and adipose)	NCBI GEO	GEO: GSE64770
Gonadectomized RNA-seq data	NCBI GEO	GEO: GSE112947
Experimental Models: Organisms/Strains		
C57BL/6J, male and female, 8 weeks old	Jackson Laboratories	Stock# 000664
A/J, male and female, 8 weeks old	Jackson Laboratories	Stock# 000646
C3H/HeJ, male and female, 8 weeks old	Jackson Laboratories	Stock# 000659
Lypla1 ^{tm1a(KOMP)^{Wtsi}}	KOMP Repository	Project# CSD23342
Oligonucleotides		
Mitochondrial primers (Method Details)	This paper	N/A
qPCR primers (Method Details)	This paper	N/A
Software and Algorithms		
WGCNA	https://cran.r-project.org/	N/A
R software environment for analyses	https://www.r-project.org/	N/A
GCTA	http://cnsgenomics.com/software/gcta/gcta_1.26.0_src.zip	N/A
SaVanT	http://newpathways.mcdb.ucla.edu/savant	N/A
DESeq2	https://bioconductor.org/packages/release/bioc/html/DESeq2.html	N/A
pheatmap	https://cran.r-project.org/	N/A
DAVID	https://david.ncifcrf.gov/	N/A

CONTACT FOR REAGENT AND RESOURCE SHARING

Further information and requests for resources and reagents should be directed to and will be fulfilled by the Lead Contact, Aldons J. Lusis (jlusis@mednet.ucla.edu).

EXPERIMENTAL MODEL AND SUBJECT DETAILS

Animals

All of the mice strains included in the HMDP study were obtained from The Jackson Laboratory and have been described in detail ([Bennett et al., 2010](#)). The strains of mice included in this study is listed in [Table S2](#). The experimental design of the HF/HS feeding study has been described previously ([Parks et al., 2013](#)). Briefly, the mice were maintained on a chow diet (Ralston Purina Company) until 8 weeks of age before switching to a HF/HS (Research Diet-D12266B, New Brunswick, NJ) diet for 8 weeks. The gonadectomy and ovariectomy study is described in detail ([Parks et al., 2015](#)). The mice were either maintained on chow diet for 16 weeks or on chow diet until 8 weeks of age, or then switched to a HF/HS diet for 8 weeks. The mice were gonadectomized, gonadectomized with testosterone implantation, or sham operated under isoflurane anesthesia at 6 weeks of age. Mice were housed in rooms with a 14-hr

light/10-hr dark cycle (light is on between 6 a.m. and 8 p.m.) at a temperature of 25 degrees. On the day of experiment, mice from both studies were sacrificed after a 4 h fast between 10.30 a.m. and noon. We did not assess the reproductive phase of the females as this was not feasible in such a large study. In mice that received hormonal replacement at time of surgery, a small incision was made at the base of the back of the neck. A 5 mg pellet of 5 α -dihydrotestosterone 90-day release (innovative Research of America, FL) was inserted and the incision closed.

Principle component analysis was performed on gonadectomized liver samples using prcomp (R Studio). The contribution of each gene to total variances for principle components 1 and 2 were obtained and shown on [Figure S3](#). To ask whether the observed shifts in male liver along the PC axes following gonadectomy in [Figure 5B](#) were due to the presence of the hormone itself, gonadectomized males were administered testosterone (DHT) or vehicle. Gene expression from the top drivers of PC1 were measured in liver using qPCR ([Figure 5](#)) and compared between groups. Of the seven top contributing genes measured, 5 were significantly reversed upon hormone administration. These data suggest that the total shifts in liver gene expression following gonadectomy were substantially impacted by testosterone levels.

This study was performed in strict accordance with the recommendations in the Guide for the Care and Use of Laboratory Animals of the National Institutes of Health. All of the animals were handled according to approved institutional animal care and use committee (IACUC) protocols (#92-169) of the University of California at Los Angeles. The animal procedures were approved by the Institutional Care and Use Committee at University of California, Los Angeles.

METHOD DETAILS

Phenotype-Phenotype Correlations

Since the HMDP mice differ in size, it is likely that many metabolic measurements could simply reflect such differences. To correct for this, we have adjusted phenotypes using kidney weight, which tends to be relatively invariant among the strains.

For every pairwise combination of phenotypes, in each sex, we calculated biweight midcorrelation (a robust, and less sensitive to outliers, alternative to Pearson correlation) using bicorAndPvalue function of the WGCNA package. In addition to the theoretical p-value returned by the bicorAndPvalue, we performed 1000 permutations of each phenotype pair (total of 1,682,000 permutations). The male and female cross phenotype correlation matrix was visualized with R function 'pheatmap'.

RNA Library Preparation and Sequencing

Upon sacrifice, tissues were instantly frozen in liquid nitrogen. Frozen tissues were homogenized in Qiazol, and following chloroform phase separation RNA was prepared from the pink phase using Qiagen miRNAeasy kits as per original protocol. Total RNA quality was validated with BioANALyzer (all samples had RIN>8). Global gene expression in liver and gonadal adipose tissue from the HMDP strains were analyzed using Affymetrix HT_MG430A arrays, and data were filtered as described ([Parks et al., 2013](#)). RNA libraries were prepared by the sequencing facility at the UCLA Neurosciences Genomics Core using Illumina TruSeq Stranded kits v2 and paired-end sequencing. Reads were aligned using STAR 2.5.2b, mm10 genome and GENCODE M11 transcript annotation. First, we built a genome index that included the transcript annotation with k-mers adjusted to read length -1 (as suggested by STAR manual). Mapping was performed with 48Gb of RAM, and 12 processors. Reads-per-gene tables were generated as part of STAR output (<https://github.com/alexdobin/STAR>) and DESeq2 (<https://bioconductor.org/packages/release/bioc/html/DESeq2.html>) was used for differential expression analysis. Differential expression analysis was run in a multi-variate mode on each tissue separately, testing for both sex and diet effects. Plotting of PCA was carried out directly as part of DESeq2 analysis using "plotPCA" function.

Tissue Deconvolution

Cell composition of adipose was assessed by deconvolution using gene expression data from the HMDP or gonadectomy studies with SaVanT (<http://newpathways.mcdub.ucla.edu/savant>) using cell type signatures from the Human Primary Cell Atlas.

Heritability

Heritabilities and their standard errors were calculated using the software package GCTA (Genome-wide Complex Trait Analysis) ([Yang et al., 2011](#)). The source code for the version we used is publicly available at http://cnsgenomics.com/software/gcta/gcta_1.26.0_src.zip.

Genome-Wide Association Analyses

Association analysis is a method of determining which regions of the genome have effects on a quantitative trait. In a panel of inbred mice such as the HMDP, the shared ancestry of many of the strains used results in population structure. A naïve approach to association analysis would ignore this structure and produce artificially low p-values since the contribution of the shared genetic background to the phenotypic values would mistakenly be attributed to the particular variant being tested for association. Therefore, mapping of each trait in each sex was performed using Fast-LMM (Factored spectrally-transformed Linear Mixed Models) with correction for population structure as previously described ([Hasin-Brumshstein et al., 2016](#); [Orozco et al., 2012](#); [Parks et al., 2015](#)). The regression equation used in this method includes a term that accounts for the genetic relatedness of all the individuals tested. The genetic relatedness matrix (GRM) is constructed from all of the SNPs tested, with the refinement that when testing SNPs on a

particular chromosome N for association, all SNPs from chromosome N are excluded from the GRM. This prevents any SNP from incorrectly being used in the regression equation twice, which would result in potential false negative results. SNPs with minor allele frequencies below 5% or missing genotype frequencies greater than 10% were excluded, leaving approximately 200,000 SNPs (Rau et al., 2015) used in the final analysis. Genotypes for these SNPs were obtained using the Mouse Diversity Array (Yang et al., 2009).

Lyplal1 Studies

Sperm from *Lyplal1*^{tm1a}(KOMP)^{Wtsi} C57BL/6N mice were obtained from the University of California Davis KOMP Repository Knockout Mouse Project and mice were rederived at University of California Los Angeles. Female and male mice were maintained on a chow diet (Ralston Purina Company) until 8 weeks of age when they were given a HF/HS diet (Research Diets-D12266B, New Brunswick, NJ) with the following composition: 16.8% kcal protein, 51.4% kcal carbohydrate, 31.8% kcal fat. Total body fat mass and lean mass were measured by magnetic resonance imaging using Bruker Minispec before the start of the HF/HS diet and thereby biweekly, as described (Parks et al., 2013). After 8 weeks on the HF/HS diet, mice were sacrificed after a 4-hr fast. Blood was collected by retro-orbital bleeding under isoflurane anesthesia. Subcutaneous, mesenteric, retroperitoneal and gonadal adipose tissues were carefully dissected and weighed from a subset of the animals. Plasma, liver and adipose tissues were frozen immediately after dissection in liquid nitrogen and stored at -80°C until analysis.

Mitochondrial DNA Content

Mitochondrial DNA content was measured as described previously (Rooney et al., 2015; Venegas and Halberg, 2012; Vergnes et al., 2011). Briefly, total (mitochondrial and nuclear) DNA from gonadal adipose tissue was isolated by phenol/chloroform/isoamyl alcohol extraction. Both mitochondrial and nuclear DNA were amplified by quantitative PCR with 25 ng of total DNA using primers in the D-loop region (AATCTACCATCCTCCGTGAAACC; TCAGTTTAGCTACCCCAAGTTTAA) and Tert gene (CTAGCTCATGTGT CAAGACCCTCTT; GCCAGCACGTTTCTCTCGTT), respectively. Mitochondrial DNA content, normalized to nuclear DNA, was calculated using the equation $2 \times 2^{-\Delta\text{Ct}}$ ($\Delta\text{Ct} = \text{D-loop Ct} - \text{Tert Ct}$) and then reported as relative units of corresponding female groups.

Mitochondrial Bioenergetics

Mitochondria were isolated from fresh tissues and immediately used in an XF24 Analyzer (Seahorse Bioscience) as previously described (Vergnes et al., 2016). Briefly, the mitochondrial pellet was isolated by dual centrifugation at 800g and 8000g. 25 μg mitochondria were seeded per well by centrifugation. Oxygen consumption rate (OCR) was measured in the presence of 10 mM succinate (complex II substrate) and 2 μM rotenone (complex I inhibitor), and after sequential addition of 4 mM ADP (Complex V substrate), 2.5 $\mu\text{g}/\text{ml}$ oligomycin (Complex V inhibitor), 4 μM FCCP (mitochondrial uncoupler) and 4 μM antimycin A (Complex III inhibitor). OCR was normalized per μg mitochondrial protein. Maximal respiration represents the response to FCCP. Coupled and uncoupled respiration rates were the oligomycin-sensitive and the difference between rates observed after the addition of oligomycin and antimycin A, respectively.

Mitochondrial Immunoblot Procedures and Analyses of Function

Mitochondria prepared for mitochondria bioenergetics as described above were lysed in Whole Cell Extraction buffer (WCE) containing 62.5 mM Tris-HCl (pH 6.8), 2% (wt/v) Sodium dodecyl sulfate, and 10% glycerol (Seldin et al., 2017). Samples were then heated and diluted 1:5 in water, and protein content measured using a BCA protein assay kit (Pierce). 10 μg samples were denatured in 4x LDS loading buffer (Life Technologies) with 10x reducing agent (Life Technologies) at 99°C for 20 min, loaded at 10 $\mu\text{L}/\text{well}$ into 4-12% Bis-Tris gels (Invitrogen) and separated out at 130 volts for 2 hr. Protein was then transferred to PVDF membranes (Immobilon) for 1.5 hr at 35 volts. Following transfer, membranes were washed with TBST, and then blocked in 5% skim milk (Gibco) in TBST for 1 hr at room temperature. Membranes were then placed in a primary antibody cocktail for total OxPhos complex cocktail (Abcam, # ab110413, 1:2000) or TOM20 (Santa Cruz, # sc-17764 1:500) on a shaker overnight at 4°C . The following day, membranes were washed 3X in TBST then placed in secondary antibodies (1:2000) for 1hr at room temperature. Blots were then washed 3X in TBST and placed in Amersham ECL detection solution (GE health sciences). Blots were imaged using IMAGER and bands were quantified using Image J Software.

Immunohistochemistry

Gonadal fat samples were dissected and subsequently fixed and stored in 4% paraformaldehyde. After dehydration, tissues were embedded in paraffin and cut into 5 μm slices. Immunohistochemical staining was performed on a Discovery XT automated stainer (Ventana, Medical Systems) using rabbit anti-UCP1 antibody (1:1500; ab10983, Abcam). Signal detection was performed using the diaminobenzidine as a chromogen (Ventana Medical Systems). Images obtained by UCP1 and H&E staining were analyzed using the commercially available image analysis software Definiens Developer XD2.1 (Definiens AG; München, Germany). For this purpose, all stained slides were scanned at 20x objective magnification using a Mirax Desk digital slide scanner (Carl Zeiss MicroImaging, Munich, Germany), and the resulting images were imported into image analysis software. A specific rule set was defined to detect the stained tissue area (UCP1) or the adipocytes (H&E) within each defined region. The quantified parameter was the percentage of the UCP1 stained area related to the defined tissue area. For H&E staining the calculated parameter was the mean size of the adipocytes.

QUANTIFICATION AND STATISTICAL ANALYSIS

Statistical Analyses

Phenotype-phenotype correlations: Correlations were calculated in R with `bicor` function from WGCNA (<https://cran.r-project.org/web/packages/WGCNA/index.html>). `Bicor` calculates biweight mid-correlations, which are a robust (less sensitive to outliers) alternative to Pearson correlations. Permutations were carried out in R, by randomizing one of the phenotypes, then calculating the p-value and correlation on the permuted data. For each phenotype-phenotype pair we obtained 1,000 randomized p values. Distributions of randomized p values were very similar between all pairs of phenotypes, thus we used the combined distributions of p values to assess significance thresholds.

Microarrays: gene expression in adipose and liver of HMDP mice was measured with microarrays, as described in Parks et al. (2013). Array data was normalized and adjusted for batch effects using RMA - a standard processing package for Affymetrix microarray data. Outlier samples (one in adipose and one in liver) and strains that were not present in all 4 data-sets were removed from further analysis. We then filtered out: 1. Low quality probes, as annotated in Affymetrix annotation file HT_MG-430A.na36.annot.csv (downloaded from company website). 2. Low expressed probes: we required expression > 4 in 70 or more strains in either sex. Differential expression analysis was carried out with R package “limma” (<http://bioconductor.org/packages/limma/>) at the probe level, using design model of $\sim \text{strain} + \text{sex}$.

Gene enrichment analysis was carried out using DAVID (<https://david.ncifcrf.gov/>). For background expression we used tissue specific list of expressed genes, the same as was used with for differential expression. The threshold for significance was $p < 0.01$.

Unless otherwise noted, values presented are expressed as means \pm SEM. The two-sample Student's t-test was used to examine the difference between the two groups. All analyses were performed using R 3.1.0 (Vienna, Austria), and p values < 0.05 were considered statistically significant.

The statistical parameters can also be found in the figure legends.

DATA AND SOFTWARE AVAILABILITY

The accession numbers for the expression arrays and RNA-seq data used in this study are GEO: GSE64770 (HMDP expression arrays [liver and adipose]) and GEO: GSE112947 (Gonadectomized RNA-seq data).

Supplemental Information

Gene-by-Sex Interactions in Mitochondrial

Functions and Cardio-Metabolic Traits

Frode Norheim, Yehudit Hasin-Brumshtein, Laurent Vergnes, Karthickeyan Chella Krishnan, Calvin Pan, Marcus M. Seldin, Simon T. Hui, Margarete Mehrabian, Zhiqiang Zhou, Sonul Gupta, Brian W. Parks, Axel Walch, Karen Reue, Susanna M. Hofmann, Arthur P. Arnold, and Aldons J. Lusis

Table S1. Sex differences in clinical traits. Related to Figure 1

Trait	p-value*	FDR-adjusted p-value†	Average value (males)	Average value (females)	Top significant QTL in males	Top significant QTL in females
Body fat % growth	1.467E-03	2.674E-03	144.013	107.591	chr13:91591879 (6.74e-11)	chr1:5711829 (5.91e-07)
Body fat response	5.312E-02	7.382E-02	16.361	14.409	chr14:11525491 (7.26e-08)	chr7:69214973 (2.01e-07)
Body fat response (normalized to kidney weight)	7.067E-03	1.136E-02	91.348	111.671	chr7:127215079 (1.37e-06)	chr17:43340215 (7.14e-07)
Corpuscular hemoglobin (g/dl)	8.695E-01	8.803E-01	31.871	31.795	chr7:102226175 (3.68e-90)	chr7:102949492 (2.89e-112)
Fat mass % growth	1.088E-02	1.621E-02	287.358	226.789	chr16:93301822 (4.33e-11)	chr10:27777268 (3.09e-06)
Fat mass 0 wks diet	2.032E-01	2.314E-01	3.600	3.305	chr14:14239575 (2.43e-08)	
Fat mass 0 wks diet (normalized to kidney weight)	2.969E-04	6.406E-04	19.784	25.394	chr14:13158638 (5.28e-07)	
Fat mass 8 wks	5.470E-03	9.344E-03	12.273	10.239	chr7:127290257 (4.43e-09)	chr7:66856049 (1.32e-07)
Fat mass 8 wks (normalized to kidney weight)	3.986E-02	5.635E-02	67.837	78.347	chr7:127065727 (3.65e-06)	chr17:66421918 (3.07e-06)
Fat mass response	4.087E-03	7.130E-03	8.673	6.934	chr7:127290257 (2.35e-08)	chr7:66856049 (2.14e-07)
Fat mass response (normalized to kidney weight)	2.442E-01	2.743E-01	48.052	52.953		chr17:66421918 (3.75e-07)
Food intake average	3.195E-05	8.186E-05	3.144	2.829	chr1:178298128 (5.69e-14)	chr1:172751095 (1.31e-09)
Food intake average (normalized to kidney weight)	1.659E-13	1.134E-12	17.265	22.132	chr17:12406998 (5.5e-07)	
Food intake day 1	8.459E-03	1.334E-02	3.230	2.990	chr1:178298128 (3.63e-16)	chr1:172742472 (1.58e-09)
Food intake day 1 (normalized to kidney weight)	3.218E-13	2.030E-12	17.736	23.366	chr1:178465794 (1.41e-06)	
Food intake day 2	2.481E-04	5.498E-04	3.111	2.779	chr1:175768248 (4.39e-07)	chr1:177553977 (7.59e-08)
Food intake day 2 (normalized to kidney weight)	1.536E-10	5.998E-10	17.049	21.737	chr17:11880850 (7.18e-07)	
Food intake day 3	7.242E-05	1.697E-04	3.175	2.845	chr1:175789094 (7.88e-09)	
Food intake day 3 (normalized to kidney weight)	9.882E-11	4.051E-10	17.680	22.383		chr1:90644249 (1.93e-06)
Food intake day 4	5.876E-06	1.721E-05	3.006	2.564	chr9:57610867 (1.77e-06)	
Food intake day 4 (normalized to kidney weight)	8.038E-07	2.441E-06	16.831	20.444		chr5:104948585 (1.29e-06)
Gonadal fat weight	6.739E-02	8.771E-02	1.501	1.325	chr7:74534452 (2.79e-07)	chr17:67199420 (1.39e-07)
Gonadal fat weight (normalized to kidney weight)	8.807E-03	1.363E-02	8.314	10.073	chr7:74534452 (3.43e-07)	
Granulocytes (thousands/ul)	5.099E-05	1.230E-04	1.703	1.382	chr12:49333533 (1.80e-06)	chr11:26100680 (1.79e-06)
Granulocytes (% of white cells)	1.146E-01	1.423E-01	21.722	20.659	chr6:43884850 (1.01e-08)	
HDL	7.534E-13	4.412E-12	166.850	121.555	chr1:168279177 (2.12e-06)	chr1:171208377 (1.90e-06)
Heart weight	8.886E-15	7.287E-14	0.152	0.120	chr17:87783921 (1.96e-06)	
Heart weight (normalized to kidney weight)	3.093E-05	8.182E-05	0.831	0.927		
Hematocrit (%)	8.271E-01	8.478E-01	43.844	43.645	chr7:102226175 (1.38e-24)	chr7:102152386 (3.90e-34)
Hemoglobin (g/dl)	4.899E-01	5.217E-01	13.817	13.693	chr14:52392537 (1.52e-07)	
HOMA-IR	5.519E-12	3.017E-11	64.169	21.507	chr9:104018744 (1.50e-07)	chr15:54129738 (1.60e-06)
Kidney weight	7.062E-27	1.158E-25	0.186	0.131	chr7:107313081 (5.91e-07)	chr10:90146088 (5.04e-07)
LDL	2.246E-04	5.115E-04	43.185	33.166	chr9:67247812 (7.28e-07)	
Lean mass 0 wks HF diet	2.910E-32	7.955E-31	21.686	17.589	chr1:178551913 (4.20e-07)	chr4:101456134 (5.84e-07)
Lean mass 0 wks HF diet (normalized to kidney weight)	5.259E-09	1.797E-08	119.642	136.483	chr17:11880850 (2.35e-09)	
Lean mass 8 wks diet	2.101E-30	4.307E-29	26.210	21.201	chr13:8190622 (1.14e-08)	chr17:48931420 (1.31e-09)
Lean mass 8 wks diet (normalized to kidney weight)	1.903E-09	6.784E-09	144.255	164.151	chr17:10562672 (2.6e-11)	chr18:70827226 (1.54e-06)
Liver phospholipids	1.185E-38	4.860E-37	15.277	10.094		chr4:64250239 (3.60e-06)
Liver total cholesterol	2.000E-08	6.561E-08	3.550	2.747	chr1:178551913 (1.66e-06)	chr5:64528298 (3.52e-07)
Liver triglycerides	1.148E-05	3.245E-05	82.707	50.855	chr9:104875641 (1.56e-06)	
Liver unesterified cholesterol	1.213E-42	9.951E-41	2.394	1.404	chr11:92030285 (2.55e-06)	chr4:53135994 (1.52e-06)
Liver weight	3.832E-07	1.208E-06	1.435	1.138	chr7:117236190 (3.43e-09)	chr17:48914545 (7.24e-07)
Liver weight (normalized to kidney weight)	6.118E-03	1.024E-02	7.834	8.732	chr17:24082554 (1.64e-08)	chr17:32378517 (1.73e-06)
Lung weight	5.852E-02	7.867E-02	0.181	0.172	chr10:125503808 (2.90e-06)	chr19:51166266 (3.78e-06)
Lung weight (normalized to kidney weight)	7.466E-19	8.746E-18	0.994	1.332		
Lymphocyte (% of white cells)	1.521E-01	1.807E-01	71.186	72.331	chr6:43884850 (1.20e-09)	chr7:144676202 (2.95e-06)
Lymphocytes (thousands/ul)	6.982E-03	1.136E-02	5.859	5.060	chr12:82586480 (3.37e-06)	chr17:45252677 (4.67e-07)
Mean corpuscular hemoglobin (pg)	1.378E-01	1.686E-01	14.344	14.505	chr8:87339300 (1.95e-06)	
Mean corpuscular volume (fl)	4.708E-01	5.147E-01	45.461	46.006	chr7:103866951 (1.32e-65)	chr7:104230845 (1.22e-61)
Mean platelet volume (fl)	9.656E-02	1.237E-01	6.229	6.337	chr7:104239041 (1.71e-17)	chr7:104239041 (9.24e-08)
Mesenteric fat weight	4.667E-04	9.333E-04	0.629	0.481	chr14:96517733 (6.59e-07)	chr17:47456894 (6.89e-08)
Mesenteric fat weight (normalized to kidney weight)	4.834E-01	5.216E-01	3.466	3.665		chr7:67542847 (1.78e-07)

Trait	p-value*	FDR-adjusted p-value†	Average value (males)	Average value (females)	Top significant QTL in males	Top significant QTL in females
Monocytes (thousands/ul)	1.269E-02	1.858E-02	0.611	0.537	chr18:55974695 (2.71e-08)	
Monocytes (% of white cells)	6.623E-01	6.875E-01	7.077	6.981	chr6:48809036 (6.10e-07)	
Plasma esterified cholesterol	2.455E-10	9.150E-10	164.203	122.213	chr9:67247812 (2.95e-08)	chr1:172429451 (3.02e-06)
Plasma free fatty acids	6.373E-01	6.699E-01	36.574	36.997		
Plasma glucose	3.710E-05	9.218E-05	271.546	224.914	chr7:49397123 (3.88e-08)	chr11:112944793 (3.77e-07)
Plasma glycerol	1.444E-01	1.741E-01	65.385	68.169		
Plasma insulin	3.700E-14	2.758E-13	3797.110	1560.821	chr1:174036719 (3.01e-07)	chr1:172489036 (3.21e-07)
Plasma total cholesterol	4.093E-11	1.865E-10	209.712	153.794	chr9:67247812 (1.36e-08)	chr17:50324480 (2.14e-06)
Plasma triglycerides	4.599E-04	9.333E-04	59.692	41.745	chr7:76638409 (6.08e-09)	chr7:66072499 (1.28e-14)
Plasma unesterified cholesterol	2.958E-11	1.427E-10	45.622	31.582		chr13:109891309 (1.01e-07)
Platelet counts (thousands/ul)	1.558E-03	2.777E-03	300.890	264.543		
Red blood cells (millions/ul)	1.898E-01	2.207E-01	9.646	9.478		
Red cell distribution width (fl)	9.300E-01	9.300E-01	29.595	29.554	chr7:104239041 (3.44e-43)	chr7:104571898 (3.55e-44)
Red cell distribution width (%)	2.554E-02	3.673E-02	17.480	17.084	chr7:102142368 (3.86e-16)	chr7:104230845 (9.22e-21)
Retroperitoneal fat weight	3.959E-16	3.607E-15	0.338	0.197		chr7:68619885 (3.07e-06)
Retroperitoneal fat weight (normalized to kidney weight)	6.765E-04	1.321E-03	1.882	1.508	chr17:3869399 (1.27e-06)	chr7:122597337 (3.42e-06)
Spleen weight	5.490E-02	7.503E-02	0.091	0.100	chr5:105602514 (1.97e-06)	
Spleen weight (normalized to kidney weight)	2.063E-18	2.115E-17	0.498	0.762	chr17:9880957 (3.89e-06)	
Subcutaneous fat weight	9.896E-03	1.503E-02	1.157	0.960		chr7:66856049 (1.26e-06)
Subcutaneous fat weight (normalized to kidney weight)	6.703E-02	8.771E-02	6.417	7.412	chr4:142202686 (5.16e-07)	
Total mass % growth	2.476E-01	2.744E-01	53.986	50.039	chr16:93301822 (1.18e-06)	chr17:43340215 (1.25e-06)
Total mass 0 wks	1.689E-19	2.308E-18	25.706	21.452	chr17:45740224 (3.42e-06)	
Total mass 0 wks (normalized to kidney weight)	7.945E-11	3.429E-10	141.762	166.228	chr17:10070612 (2.5e-09)	
Total mass 8 wks	2.343E-11	1.201E-10	39.450	32.303	chr13:8190622 (4.63e-09)	chr17:45740224 (1.27e-07)
Total mass 8 wks (normalized to kidney weight)	2.978E-05	8.139E-05	217.403	249.126	chr17:10065097 (9.6e-09)	
Total mass growth	3.998E-04	8.407E-04	13.736	10.851	chr9:92273734 (3.68e-07)	chr17:48495769 (3.75e-07)
Total mass growth (normalized to kidney weight)	1.911E-01	2.207E-01	75.625	82.899	chr4:143041959 (8.42e-07)	chr7:66494857 (1.69e-06)
Visceral fat weight	1.196E-03	2.281E-03	2.466	2.003	chr13:8190622 (1.01e-07)	chr17:67197249 (1.38e-07)
Visceral fat weight (normalized to kidney weight)	1.038E-01	1.310E-01	13.647	15.245	chr7:73942680 (1.45e-06)	
White blood cells (thousands/ul)	1.406E-03	2.621E-03	8.168	6.972		chr17:45252677 (3.85e-06)

* using two-sample Student's t-test

† adjusted using Benjamini-Hochberg method

Table S3. Enrichment analysis (DAVID) results for adipose. Related to Figure 2

Category	Term	Count	%	P-Value	Benjamini
UP_KEYWORDS	Transit peptide	264	7.2	3.70E-30	1.80E-27
GOTERM_CC_DIRECT	mitochondrion	652	17.8	1.00E-25	1.10E-22
UP_SEQ_FEATURE	transit peptide:Mitochondrion	238	6.5	1.90E-26	1.30E-22
UP_KEYWORDS	Mitochondrion	443	12.1	8.10E-25	2.00E-22
UP_KEYWORDS	Mitochondrion inner membrane	132	3.6	3.00E-15	4.90E-13
KEGG_PATHWAY	Oxidative phosphorylation	74	2	6.90E-15	2.00E-12
GOTERM_CC_DIRECT	mitochondrial inner membrane	187	5.1	1.20E-14	6.60E-12
UP_KEYWORDS	Electron transport	63	1.7	2.50E-13	3.10E-11
UP_KEYWORDS	Respiratory chain	41	1.1	5.60E-13	5.50E-11
GOTERM_CC_DIRECT	respiratory chain	40	1.1	2.10E-12	7.70E-10
GOTERM_CC_DIRECT	mitochondrial respiratory chain complex I	33	0.9	8.90E-11	2.40E-08
GOTERM_CC_DIRECT	mitochondrial matrix	93	2.5	1.00E-09	1.90E-07
GOTERM_CC_DIRECT	extracellular exosome	853	23.2	9.40E-10	2.00E-07
KEGG_PATHWAY	Alzheimer's disease	83	2.3	1.10E-08	1.60E-06
KEGG_PATHWAY	Parkinson's disease	67	1.8	3.00E-08	2.20E-06
KEGG_PATHWAY	Non-alcoholic fatty liver disease (NAFLD)	79	2.2	2.30E-08	2.20E-06
KEGG_PATHWAY	Citrate cycle (TCA cycle)	25	0.7	3.50E-06	2.10E-04
GOTERM_CC_DIRECT	melanosome	54	1.5	1.50E-06	2.30E-04
KEGG_PATHWAY	Huntington's disease	80	2.2	1.10E-05	5.30E-04
UP_KEYWORDS	Tricarboxylic acid cycle	20	0.5	1.30E-05	1.10E-03
COG_ONTOLOGY	Lipid metabolism	32	0.9	9.20E-05	4.10E-03
KEGG_PATHWAY	Phagosome	64	1.7	1.20E-04	5.20E-03
UP_KEYWORDS	Disulfide bond	536	14.6	9.00E-05	5.60E-03
UP_KEYWORDS	Transport NADH dehydrogenase (ubiquinon	495	13.5	8.70E-05	6.10E-03
GOTERM_MF_DIRECT	activity	20	0.5	3.30E-06	7.60E-03
GOTERM_CC_DIRECT	mitochondrial nucleoid	30	0.8	5.90E-05	7.90E-03
KEGG_PATHWAY	Cardiac muscle contraction	25	0.7	2.30E-04	8.20E-03
UP_KEYWORDS	GTP-binding	118	3.2	1.60E-04	8.70E-03
UP_KEYWORDS	Acetylation	1038	28.3	2.00E-04	9.80E-03
UP_KEYWORDS	Ubiquinone	16	0.4	2.60E-04	1.20E-02
KEGG_PATHWAY	Propanoate metabolism	18	0.5	4.20E-04	1.20E-02
KEGG_PATHWAY	Regulation of actin cytoskeleton	79	2.2	4.10E-04	1.30E-02
GOTERM_CC_DIRECT	myelin sheath	79	2.2	1.80E-04	2.20E-02

Category	Term	Count	%	P-Value	Benjamini
GOTERM_CC_DIRECT	plasma membrane	803	21.9	2.00E-04	2.20E-02
GOTERM_BP_DIRECT	osteoblast differentiation	54	1.5	7.80E-06	2.70E-02
KEGG_PATHWAY	Tuberculosis	70	1.9	1.50E-03	3.80E-02
KEGG_PATHWAY	Fc gamma R-mediated phagocytosis	44	1.2	1.90E-03	4.60E-02
GOTERM_CC_DIRECT	membrane raft	95	2.6	5.00E-04	4.80E-02
GOTERM_BP_DIRECT	tricarboxylic acid cycle	21	0.6	7.40E-06	5.10E-02
KEGG_PATHWAY	Salmonella infection	36	1	2.30E-03	5.20E-02
UP_KEYWORDS	Hydrogen ion transport	21	0.6	1.90E-03	6.50E-02
UP_KEYWORDS	Cell membrane	505	13.8	1.80E-03	6.60E-02
UP_KEYWORDS	Receptor	225	6.1	2.10E-03	6.70E-02
UP_KEYWORDS	Membrane	1435	39.1	1.80E-03	7.10E-02
KEGG_PATHWAY	Osteoclast differentiation	55	1.5	4.00E-03	7.10E-02
KEGG_PATHWAY	B cell receptor signaling pathway	37	1	3.70E-03	7.50E-02
KEGG_PATHWAY	Carbon metabolism	56	1.5	4.00E-03	7.50E-02
UP_KEYWORDS	Glycoprotein	708	19.3	2.60E-03	7.70E-02
UP_KEYWORDS	Glucose metabolism	14	0.4	3.00E-03	8.30E-02
UP_KEYWORDS	4Fe-4S	20	0.5	3.30E-03	8.60E-02
UP_KEYWORDS	Immunity	117	3.2	3.80E-03	9.00E-02
UP_KEYWORDS	Lysosome	85	2.3	3.70E-03	9.20E-02
UP_KEYWORDS	ATP synthesis	9	0.2	4.30E-03	9.60E-02

Table S4. Enrichment analysis (DAVID) results for liver, Related to Fig 2

Category	Term	Count	%	P-Value	Benjamini
UP_TISSUE	Liver	1090	33.1	1.60E-13	4.50E-11
GOTERM_CC_DIRECT	extracellular exosome	785	23.8	3.30E-12	3.40E-09
GOTERM_CC_DIRECT	endoplasmic reticulum	399	12.1	6.80E-09	3.50E-06
UP_TISSUE	Kidney	646	19.6	1.70E-07	2.50E-05
UP_KEYWORDS	Endoplasmic reticulum	307	9.3	7.60E-08	3.70E-05
UP_TISSUE	Bone marrow	491	14.9	3.20E-06	3.10E-04
UP_KEYWORDS	Microsome	49	1.5	5.40E-06	1.30E-03
UP_TISSUE	Amnion	122	3.7	9.70E-05	6.90E-03
UP_KEYWORDS	Acetylation	943	28.6	6.20E-05	7.50E-03
UP_TISSUE	Pancreas	187	5.7	1.60E-04	9.30E-03
UP_KEYWORDS	Monooxygenase	38	1.2	6.00E-05	9.70E-03
UP_TISSUE	Placenta	226	6.9	2.20E-04	1.00E-02
GOTERM_CC_DIRECT	endoplasmic reticulum membrane	210	6.4	6.10E-05	2.10E-02
UP_KEYWORDS	Lysosome	83	2.5	2.30E-04	2.30E-02
KEGG_PATHWAY	Metabolic pathways	378	11.5	1.60E-04	2.30E-02
GOTERM_CC_DIRECT	cytosol	515	15.6	1.10E-04	2.90E-02
KEGG_PATHWAY	Retinol metabolism	31	0.9	1.00E-04	3.00E-02
UP_KEYWORDS	Oxidoreductase	175	5.3	5.00E-04	3.40E-02
UP_KEYWORDS	Lipid metabolism	125	3.8	4.30E-04	3.40E-02
GOTERM_CC_DIRECT	organelle membrane	36	1.1	2.00E-04	4.00E-02
UP_KEYWORDS	Complement pathway	16	0.5	1.20E-03	7.00E-02
UP_KEYWORDS	Steroid metabolism	31	0.9	1.40E-03	7.40E-02
UP_KEYWORDS	Alternative initiation	29	0.9	1.60E-03	7.60E-02

Supplemental Figures

Figure S1. Examples of sexually dimorphic correlations in phenotypes from highlighted sections of Figure 1A. Body fat response after 8 weeks high-fat diet versus lean mass before starting high-fat diet in A) females and B) males. Subcutaneous fat mass versus hemoglobin levels in C) females and D) males. Correlations were calculated using biweight midcorrelation (bicor) as implemented in the WGCNA R package. Shaded areas represent 95% confidence intervals from a linear model of the two traits shown.

Figure S2. Related to Figure 4. Lyplal1 mRNA in different strains of hfHMDP and relation to pathways in adipose. A) Pathway enrichment analysis of the genes correlating the most positively (red) and negatively (blue) with Lyplal1 expression in female adipose tissue. The gene ontologies were uncovered using ToppGene suite. B) Lyplal1 expression in adipose tissue of female and male mice in the HMDP. mRNA expression of Lyplal1 is highlighted for C57BL6J mice.

Figure S3. Related to Figure 5 and Figure 6. Gonadectomy impacts global liver gene expression and adipose tissue Ucp1. A) Variable contribution for each gene to PC1 and PC2 in gonadectomized liver samples from Fig 5B. B) Ucp1 mRNA expression in adipose tissue of intact and gonadectomized C57BL6J mice of both sexes related to Fig. 6D. Results are presented as mean \pm SEM. * $P < 0.05$ and ** $P < 0.01$ between gonadectomized group (GDX) and sham operated controls. P values were calculated using a students t-test (two-way).

Figure S4. Related to Figure 5. Expression levels and sex differences in eQTL genes in adipose tissue and liver. All panels show information for eQTL genes divided into groups based on overlap between tissue and sex. The groups are color coded as in color legend in Figure 5. Notches represent 95% confidence interval. A) and B) show distribution of expression level of genes in the different groups, while C) and D) show female to male fold change. Within tissue differences between groups are not significant.

Figure S5. Related to Figure 6. UCP-1 phenotype correlations in males and females. Each point represents the correlation coefficient of UCP1 to a phenotype in males (y axis) and female (x axis) hfHMDP. Correlations that are significant (corrected $p < 0.05$, permuted based) in both sexes are marked by red square, associations that are significant in one sex only are marked in blue triangles (males) and orange dots (females). Grey stars mark correlations that do not reach significance thresholds.

Figure S6. Related to Figure 6. Correlation between expression of UCP1 and beige related genes in hfHMDP. UCP1 expression in adipose tissue was correlated to four other genes implicated in adipocyte browning - Cidea, Ppargc1a, Hobx8 and Ebf2. Pink dots represent correlation in female hfHMDP while blue triangles represent correlations in male hfHMDP. Red and blue lines represent the fitted linear model for female and male data.

Figure S7. Related to Figure 7. Sex differences in mitochondrial respiration after a high-fat, high-sucrose diet. Mice were fed a high-fat, high sucrose diet (HF/HS) for 8 weeks. Mitochondria were isolated from gonadal adipose of strains (A) A/J and (B) C57BL/6J, respectively and oxidative functions tested using a Seahorse XF24 Analyzer. Different mitochondrial states were measured as described in Materials and Methods. Oxygen consumption rate (OCR) was normalized per μg mitochondrial protein ($\text{pmol/min}/\mu\text{g}$ protein). $N = 3-4$ mice per group.

Results are presented as mean \pm SEM. * $P < 0.05$ and ** $P < 0.01$ between the sexes. P values were calculated using a students t-test (two-way).

Figure S1. Examples of sexually dimorphic correlations in phenotypes from highlighted sections of Figure 1A. Body fat response after 8 weeks high-fat diet versus lean mass before starting high-fat diet in A) females and B) males. Subcutaneous fat mass versus hemoglobin levels in C) females and D) males. Correlations were calculated using biweight midcorrelation (bicor) as implemented in the WGCNA R package. Shaded areas represent 95% confidence intervals from a linear model of the two traits shown.

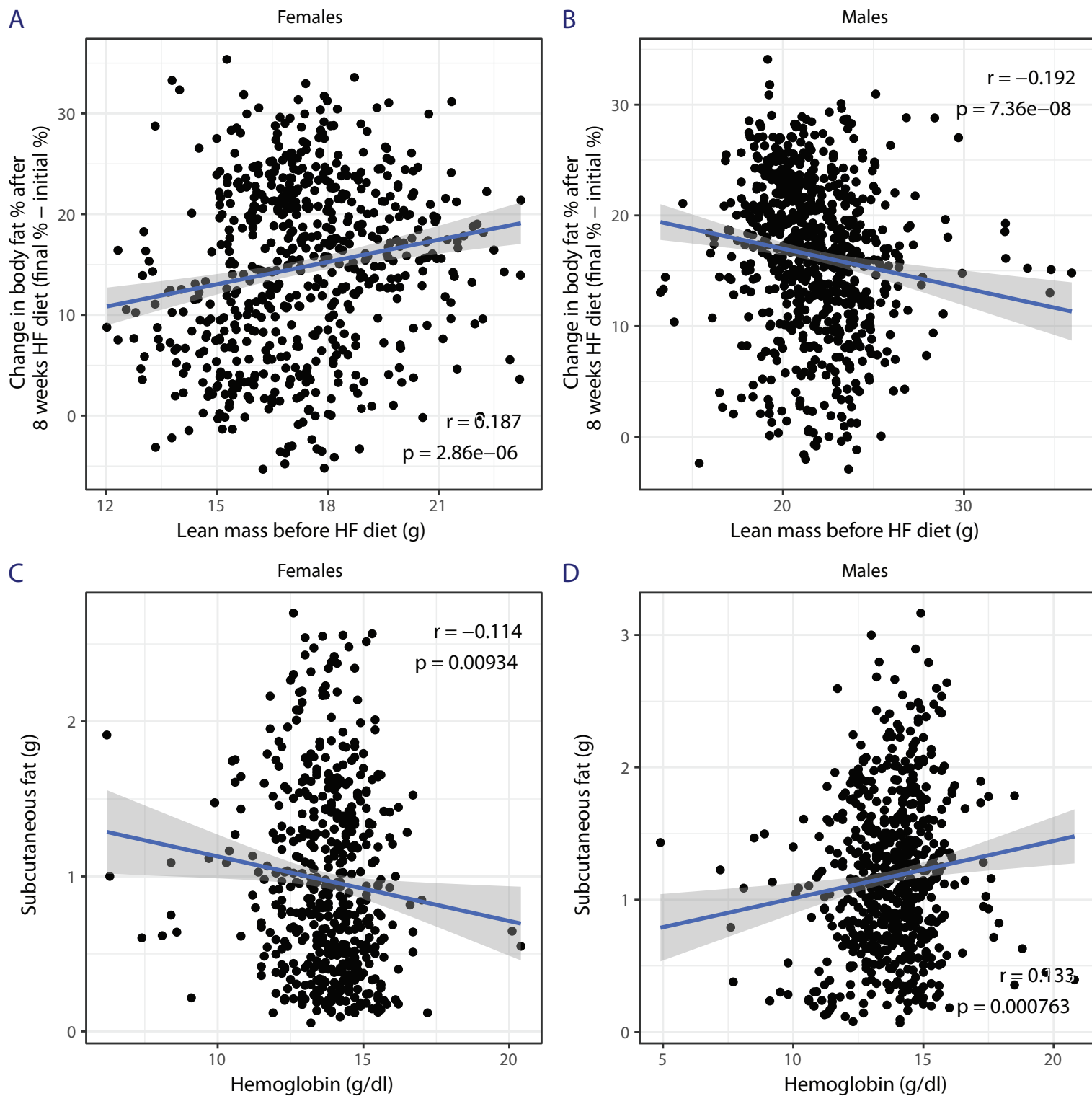


Figure S2. related to Figure 4. *Lyplal1* mRNA in different strains of HMDP and relation to pathways in adipose. A) Pathway enrichment analysis of the genes correlating the most positively (red) and negatively (blue) with *Lyplal1* expression in female adipose tissue. The gene ontologies were uncovered using ToppGene suite. B) *Lyplal1* expression in adipose tissue of female and male mice in the Hybrid Mouse Diversity Panel (HMDP). mRNA expression of *Lyplal1* is highlighted for C57BL/6J mice.

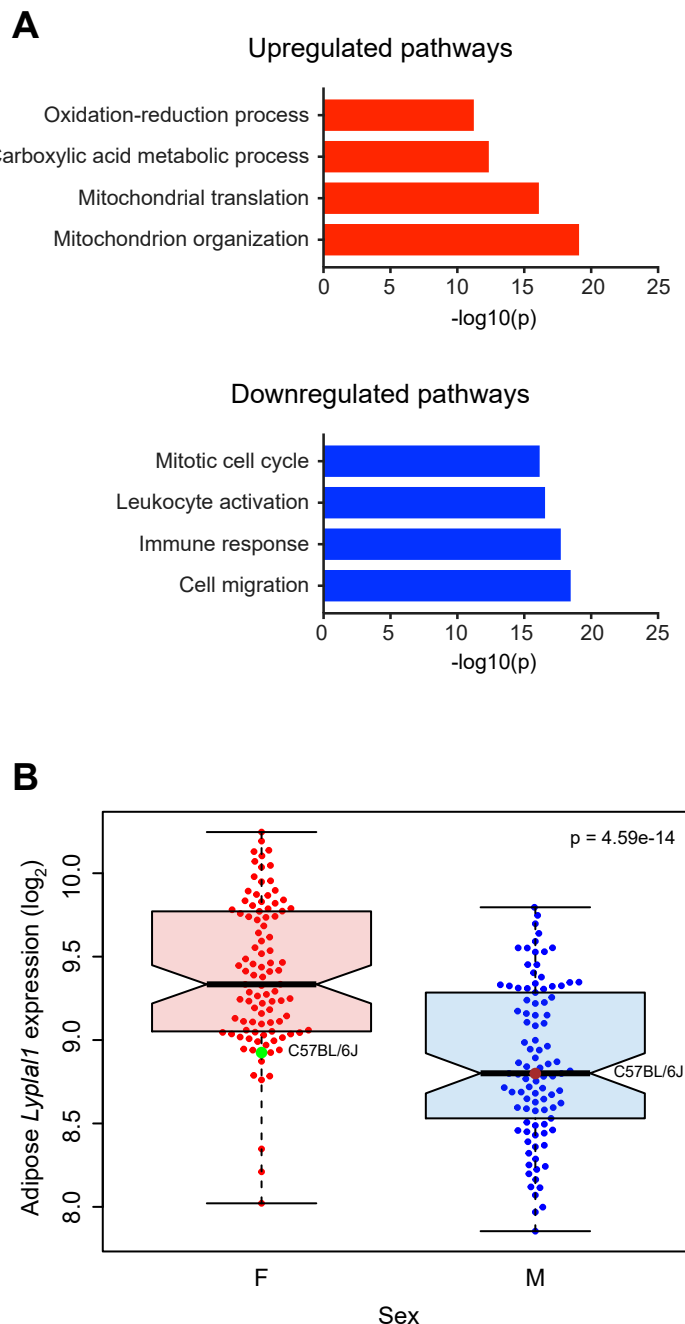


Figure S3. Related to Figure 5 and Figure 6. Gonadectomy impacts on global liver gene expression and adipose tissue Ucp1.A) Variable contribution for each gene to PC1 and PC2 in gonadectomized liver samples from Fig 5B. B) Ucp1 mRNA expression in adipose tissue of intact and gonadectomized C57BL76J mice of both sexes related to Fig. 6D. Results are presented as mean \pm SEM. *P<0.05 and **P<0.01 between gonadectomized group (GDX) and sham operated controls. P values were calculated using a students t-test (two-way).

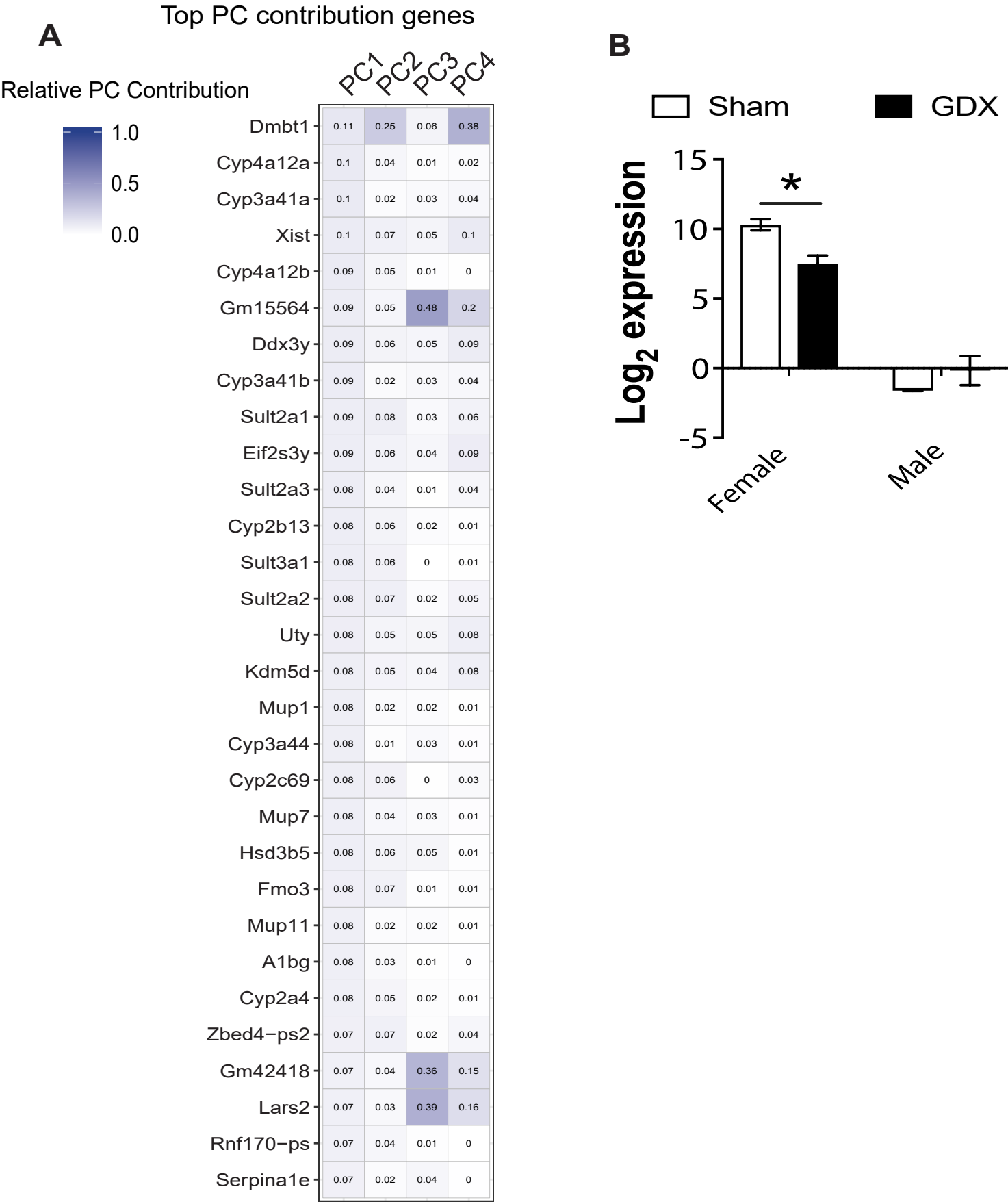


Figure S4. Related to Figure 5. Expression levels and sex differences in eQTL genes in adipose tissue and liver. All panels show information for eQTL genes divided into groups based on overlap between tissue and sex. The groups are color coded as in color legend in Figure 5. Notches represent 95% confidence interval. A) and B) show distribution of expression level of genes in the different groups, while C) and D) show female to male fold change. Within tissue differences between groups are not significant.

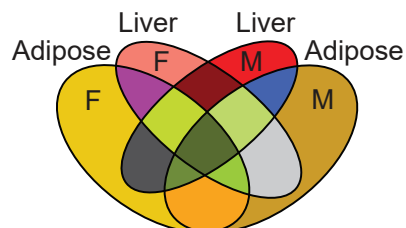
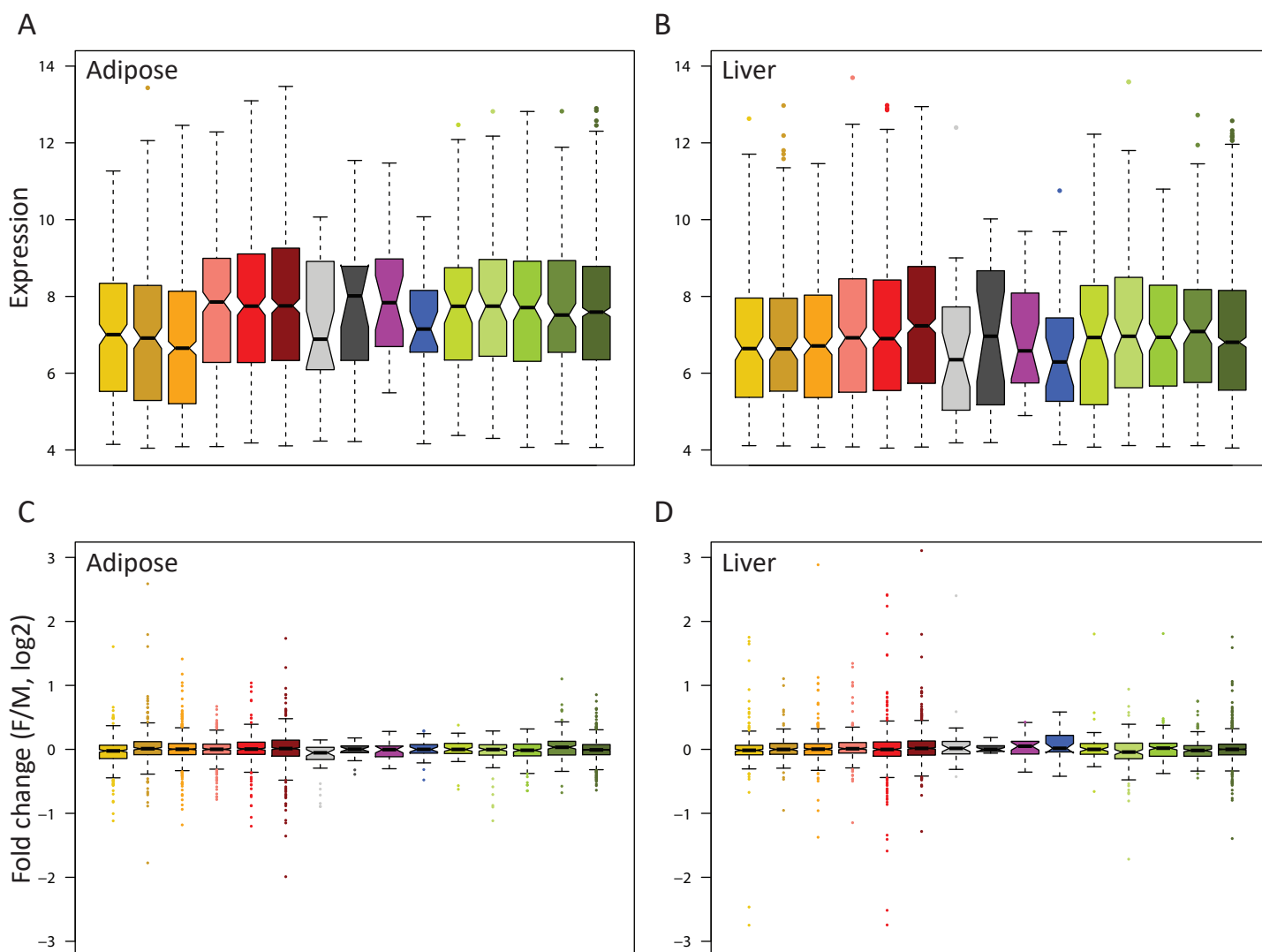


Figure S5. Related to Figure 6. UCP-1 phenotype correlations in males and females. Each point represents the correlation coefficient of UCP1 to a phenotype in males (y axis) and female (x axis) hfHMDP. Correlations that are significant (corrected $p < 0.05$, permuted based) in both sexes are marked by red square, associations that are significant in one sex only are marked in blue triangles (males) and orange dots (females). Grey stars mark correlations that do not reach significance thresholds.

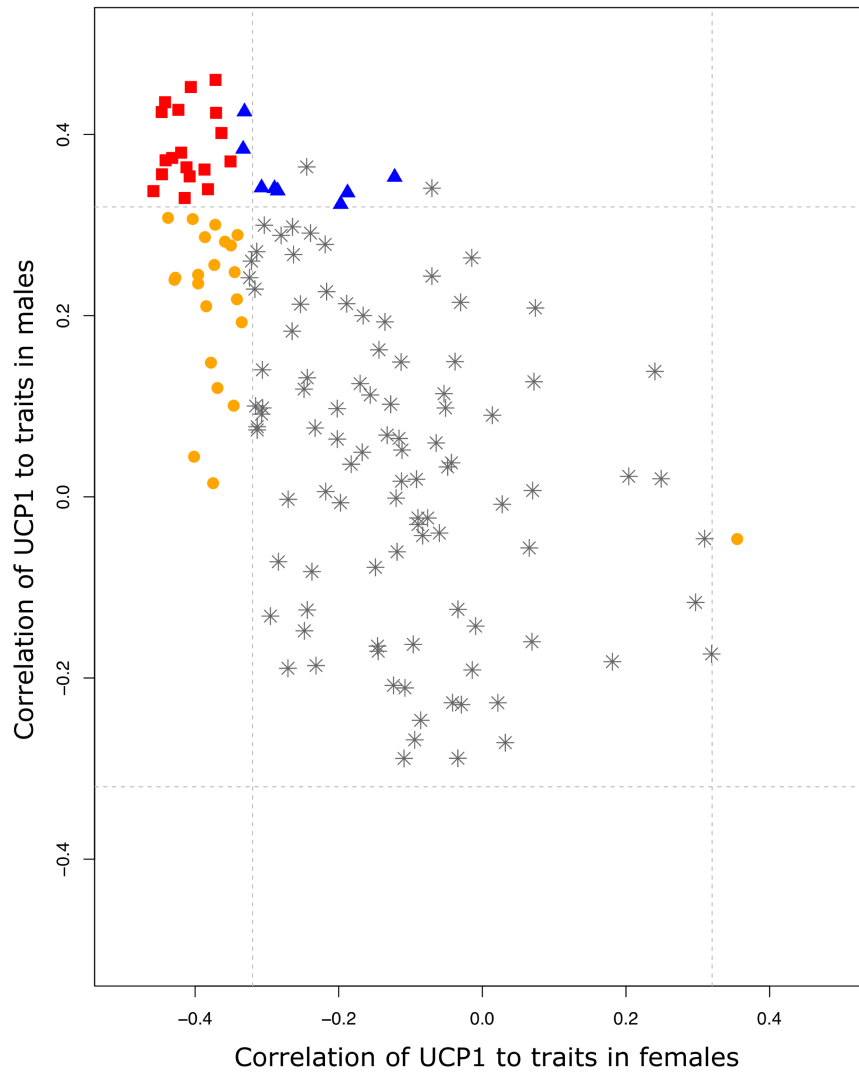


Figure S6. Related to Figure 6. Correlation between expression of UCP1 and beigeing related genes in hfHMDP. UCP1 expression in adipose tissue was correlated to four other genes implicated in adipocyte browning - Cidea, Ppargc1a, Hoxb8 and Ebf2. Pink dots represent correlation in female hfHMDP while blue triangles represent correlations in male hfHMDP. Red and blue lines represent the fitted linear model for female and male data.

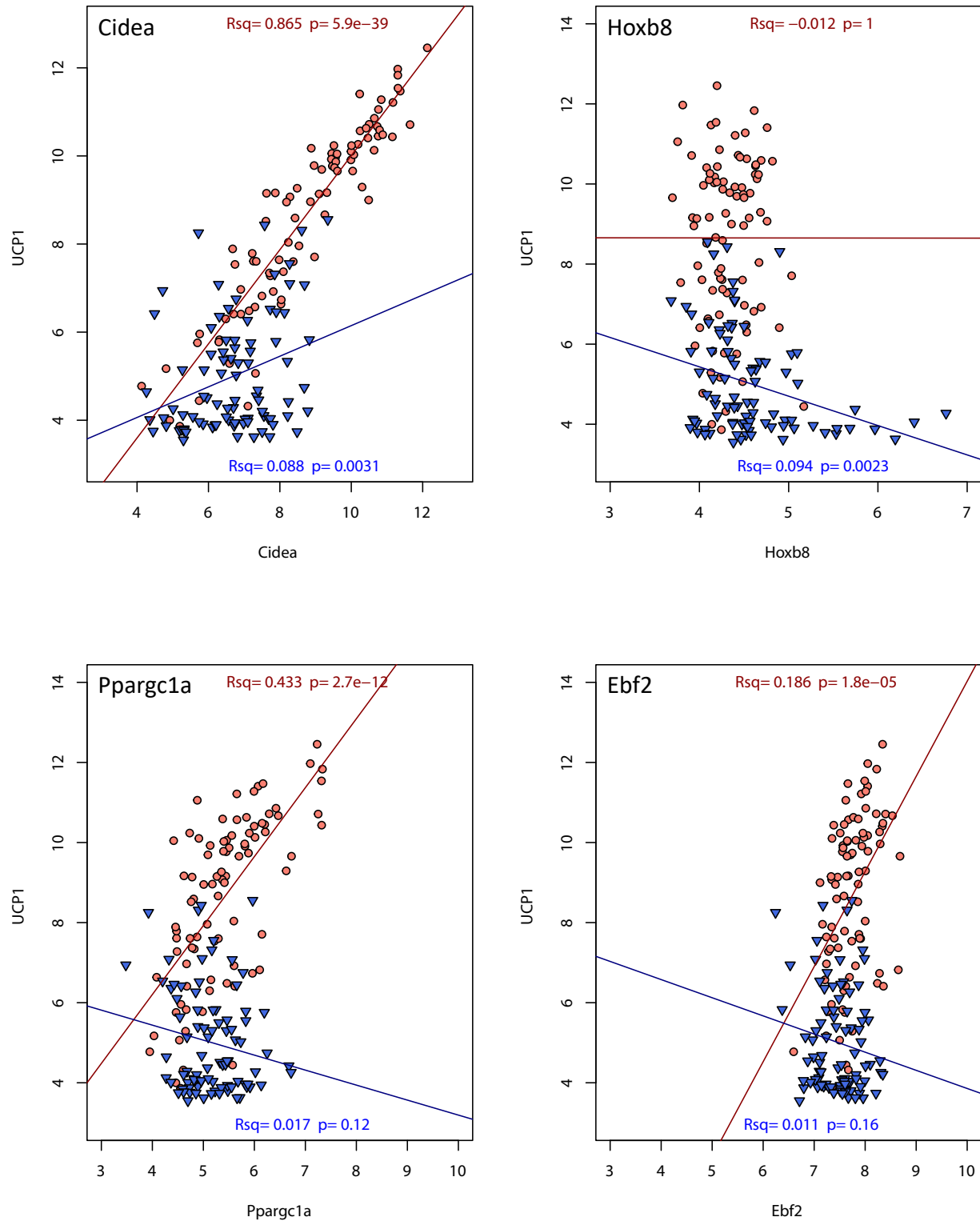


Figure S7. Related to Figure 7. Sex differences in mitochondrial respiration after a high-fat, high-sucrose diet. Mice were fed a high-fat, high sucrose diet (HF/HS) for 8 weeks. Mitochondria were isolated from gonadal adipose of strains (A) A/J and (B) C57BL/6J, respectively and oxidative functions tested using a Seahorse XF24 Analyzer. Different mitochondrial states were measured as described in Materials and Methods. Oxygen consumption rate (OCR) was normalized per μg mitochondrial protein ($\text{pmol}/\text{min}/\mu\text{g}$ protein). N = 3-4 mice per group.

